Report No. 113-30
Part VI

TWO PHASE FLOW AND HEAT TRANSFER IN POROUS BEDS UNDER VARIABLE BODY FORCES

Final Report
Part VI

By John R. McDonald and Harold R. Henry

Project Director
Harold R. Henry, Ph.D
Professor of Civil and Mineral Engineering
University of Alabama

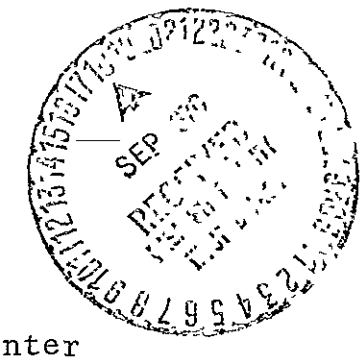

Submitted to

George C. Marshall Space Flight Center
National Aeronautics and Space Administration
Huntsville, Alabama

Contract No. NAS8-21143
University of Alabama No. 22-6560

May 1970
Bureau of Engineering Research
University of Alabama

Report No. 113-30
Part VI

TWO PHASE FLOW AND HEAT TRANSFER IN POROUS BEDS UNDER VARIABLE BODY FORCES

Final Report
Part VI

By John R. McDonald and Harold R. Henry

Project Director
Harold R. Henry, Ph.D
Professor of Civil and Mineral Engineering
University of Alabama

Submitted to

George C. Marshall Space Flight Center
National Aeronautics and Space Administration
Huntsville, Alabama

Contract No. NAS8-21143
University of Alabama No. 22-6560

May 1970
Bureau of Engineering Research
University of Alabama

TABLE OF CONTENTS

TABLE OF CONTENTS (Continued)

LIST OF FIGURES

LIST OF FIGURES (Continued)

LIST OF SYMBOLS

a	ampere
A	area, ft^2
C	specific heat, $btu/lb_m\ °F$
D	diameter, ft
F	force, lb_f
g	gravitational constant
G	mass velocity, $lb_m/hr\ ft^2$
h	height, ft
i	angle of incidence
k	thermal conductivity, btu/hr ft °F
K	effective thermal conductivity, btu/hr ft °F
L	length, ft
n	unit normal
p	pressure, lb_f/ft^2
q	heat flux, btu/hr
Q	total heat transferred, $btu/hr\ ft^2$
r	angle of refraction
Re	Reynolds Number
S	saturation
T	temperature, °F

LIST OF SYMBOLS (Continued)

v	specific volume, ft^3/lb_m
V	velocity, ft/sec
x	increment of length, ft
β	radial fraction of gas velocity
γ	radial fraction of liquid mass velocity
ε	void fraction
μ	micro
η	index of refraction
ρ	density, lb_m/ft^3
ϕ	porosity
χ	quality
ν	kinematic viscosity

Subscripts

c	conduction
e	effective
elev	elevation
f	friction
g	gas
l	liquid
m	mean
mom	momentum
o	empty channel
p	particle

LIST OF SYMBOLS (Continued)

pl	liquid specific heat
pv	vapor specific heat
R	radial
s	solid
TP	two phase
v	vapor
w	wall

PREFACE

This is Part VI of a seven part Final Report on work under Contract No. NAS8-21143 between the George C. Marshall Space Flight Center and the University of Alabama. The purpose of this entire project has been to perform analytical studies and laboratory tests related to designing an Earth-orbital experiment, i.e., perform theoretical studies, develop experimental hardware and conduct experiments for the purpose of establishing the feasibility of investigating two-phase fluid flow and heat transfer in porous beds in a reduced gravity environment.

Part VI describes the development of the breadboard packages. This includes test models of the channel for the study of liquid and its vapor and the channel for the study of liquid and foreign gas flow. Also included in the breadboard packages are pumps, motors, instrumentation and peripheral equipment for power and data recording.

In the main body of Part VI is included the description of the design, development and construction of the breadboard for the vapor-bubble experiment. Also included is an account of some fundamental experiments that were conducted on this equipment. Water and water vapor were circulated through the closed system of which the principal apparatus was a vertical channel packed with spherical glass beads.

Boiling occurred at a resistance heater located in the channel near its upstream end.

The parameters measured were liquid flowrate (obtained where one-phase flow existed); centerline and wall temperatures, wall pressures, and saturation (ratio of the volume of one-phase to the total volume of both phases) at several cross sections.

Saturation was determined by using a previously calibrated meter consisting of a light on one side of the channel and a photodiode on the other side. The amount of light transmitted through the translucent porous matrix and detected by the photodiode was a function of the number of bubble interfaces encountered by the light.

The effective thermal conductivity is estimated by considering a model for lateral heat transfer and subdividing the effects into those due to the solid matrix and those due to the two-phase mixture. The total effective conductivity calculated from experimental results is compared with that obtained by previous investigators and this comparison is presented in the results.

The experimental pressure drop through the porous bed is compared to the two-phase pressure drop through pipes obtained by earlier investigators. The correlation is remarkably close.

Appendix A describes supporting experiments which were conducted using a liquid with the same index of

refraction as the beads thus making the interior bubbles visible. Glycerine and triethylene glycol were each tested before it was decided to use water.

Appendix B describes the design, development and construction of the breadboard for the foreign gas experiment. Included is the self-contained flow system, as well as instrumentation. Fundamental experiments for the foreign-gas test setup were described in Part II.

I. INTRODUCTION

A. TWO-PHASE FLOW SYSTEMS

In two-phase flow systems one may distinguish between nonevaporative and evaporative flows. In the former, a foreign gas is introduced at some point of the flow, whereas, in the latter, the liquid vaporizes.

Evaporative flows may be further sub-divided into two classes. In the first, vaporization occurs because heat is added to the water through a fixed surface; in the second, because of a decrease in pressure. The former can be further sub-divided into two groups:

1. Pool boiling, in which the bulk liquid phase is at rest.
2. Systems in which the bulk liquid and vapor phases flow.

The latter method of producing evaporative flow is called flashing when a volume of saturated liquid is suddenly depressurized and becomes super-saturated so that vapor bubbles form rapidly.

B. HEAT TRANSFER IN PACKED BEDS WITH SINGLE-PHASE FLOW

The problem of heat flow through granulated material was discussed in a note by A. O. Sanders [19]. The author

shows, by employing the principle of similitude, that for any two heterogeneous systems of similar shape, but different in size, the ratio of effective thermal conductivities measured at any corresponding pairs of points is independent of the size and surface temperatures and is proportional to the conductivity at any specified point provided the distribution of surface temperatures and thermal conductivities are fixed (if not uniform), while varying in absolute value.

Investigations of radial heat transfer rates have followed two different methods of approach. In the first, only system boundary temperatures are measured from which heat transfer coefficients or overall effective thermal conductivities are computed. These are based upon the temperature differences of the influx and efflux gas flowing through the bed and the wall temperatures.

The second method is based upon the direct measurement of radial temperature distributions within the bed itself. Coberly and Marshall [3] and Felix and Neill [5] employed thermocouples placed across the efflux diameter of the bed, while Bunnell, Irvin, Olson, and Smith [2], Irvin, Olson, and Smith [10], and Schuler, Stallings, and Smith [21] inserted thermocouple junctions into the solid pellets making up the porous bed. Results in each case were reported in terms of effective thermal conductivities of the gas-solid bed. It was found that the resistance to heat transfer increased near the wall. Coberly and Marshall,

and Felix and Neill accounted for this by postulating that an additional lumped resistance to heat transfer existed at the wall. Bunnell, Irvin, and Schuler solved the problem by letting the effective thermal conductivity vary in a continuous manner as the wall was approached rather than postulating an additional lumped resistance at the wall.

Argo and Smith [1] proposed a method for predicting effective thermal conductivities in a packed bed in which a heated gas is flowing by summing the contribution of each mechanism by which heat is transferred radially in the bed. These mechanisms are:

1. Conduction in the gas phase.
2. Convection in the gas phase.
3. Radiation in the gas phase.
4. A mechanism accounting for the heat transfer from particle to particle by conduction, convection, and radiation.

Schotte [20] developed a correlation to predict the thermal conductivity of packed beds for various conditions of pressure, temperature, and particle size in which the effect of radiation was taken into account. Radiation heat transfer between particles should be included at high temperatures for large particles. For example, radiation becomes important for 1 mm particles at temperatures above 400°C and for 0.1 mm particles above 1500°C.

McAdams [15] suggests adding the following radiation contribution to the thermal conductivity of a bed at high temperatures:

$$k = 0.692\varepsilon D_p \frac{T^3}{10^8} \qquad (1)$$

where ε is the void fraction, D_p the particle diameter, and T the absolute temperature.

Schumann and Voss [22] developed an approximate formula which gives the thermal conductivity of a heterogeneous system, consisting of a continuous phase (air), and a disperse phase (solid particles), in terms of the conductivities of the two constituents and their concentrations. They proposed that the thermal conductivity of the system was the sum of the conductivities of each phase multiplied by its respective fractional volume or saturation. Experiments uphold the theory that the conductivity is independent of the grain size (if small compared to the system as a whole) and mode of packing.

C. HEAT TRANSFER OF TWO-PHASE FLOW IN PACKED BEDS

Heat transfer of two-phase, gas-liquid flow through packed beds is important in many chemical water treatment and heat engineering processes such as packed bed heat exchangers. Yet there is a lack of information pertaining to two-phase heat transfer in flow systems which is especially evident for low gas-liquid flow rates usually associated with bubble, slug, and froth type two-phase flows.

As late as 1965, Weekman and Myers [25] noted that there have been few, if any, serious attempts made to study heat

transfer from packed beds operating with gas-liquid flow. They studied experimentally heat transfer to beds packed with various sizes of spheres through which a two-phase air-water mixture was flowing. They predicted effective thermal conductivities ranging from 0.1 to 0.3 btu/hr ft °F using 0.255 inch diameter alumina spheres and 0.187 inch glass spheres to form their porous beds through which water and air flow rates were 5000 to 20,000 lb water/hr ft^2 and 0 to 1000 lb air/hr ft^2 respectively.

Lateral transfer is caused by a mechanical mixing through channels which are not parallel to the average direction of flow. Ranz [18] related heat transfer rates for single spheres to flow rates and pressure drops in beds packed with single particles through the application of a simple model. He considered lateral mixing to be the major contribution to the effective thermal conductivity and estimated this by considering the porous bed to consist of interconnected cells with dimensions and spacings determined by the size and shape of the particles and method of packing. Ranz utilized γ, the radial fraction of liquid mass velocity, to aid in predicting the thermal conductivity in the lateral direction. Golpalarathnam, Hoelscher, and Laddha [7] found γ to be 0.00176 for single-phase liquid flow while Weekman and Myers determined it to be 0.00174 for two-phase flow through porous beds. This remarkably close agreement implies that, for both single-phase and two phase flow, the radial fraction of the total liquid

mass velocity is the same. The effect of the gas is to impart a larger velocity to the liquid phase. This means that while the fraction of the liquid velocity in the radial direction is the same, the magnitude of the radial component will be greater for the two-phase flow.

D. PURPOSE AND SUMMARY OF EXPERIMENTAL WORK

The purpose of this research was to study experimentally two-phase flow of a single-component fluid through a porous material. It was required to design and construct a flow circuit, channel, and instrumentation to calibrate supporting equipment.

This work was part of a long range experimental research program conducted by the College of Engineering at the University of Alabama for the George C. Marshall Space Flight Center, Huntsville, Alabama. It was anticipated that in addition to establishing fundamental results, these studies and laboratory tests would be helpful in designing an earth orbital experiment; that they would lead to the development of experimental hardware for the investigation of two-phase fluid flow and heat transfer in porous beds under variable body forces in an earth-orbiting space vehicle.

The principal piece of test apparatus was a rectangular channel 3 inches by 2 inches in cross section and 24 inches long constructed of 1/4 inch thick aluminum with two viewing windows on each side. Tests were also run with the glass windows replaced with aluminum blanks. The

channel was filled with a porous bed consisting at first, of 3 mm diameter flint glass beads and later of 3 mm Pyrex glass beads. Distilled water was pumped through a closed loop system including the test channel. The vapor phase was produced by boiling at the channel entrance. Boiling was accomplished by heating the bulk liquid to a few degrees below its saturation temperature before entrance into the channel and supplying additional heat through a resistance heater located at the channel entrance.

The parameters measured were liquid flowrate (obtained where one-phase flow existed), centerline and wall temperatures, wall pressures, and saturation (ratio of the volume of one phase to the total volume of both phases) at several cross sections.

Separate experiments were conducted to calibrate meters to determine volumetric saturation at particular cross sections. Each of these meters consisted of a light on one side of the channel and a photodiode on the other side. The amount of light transmitted through the translucent porous matrix and detected by the photodiode was a function of the number of bubble interfaces encountered by the light.

A method is proposed for estimating the effective thermal conductivity of a packed-bed through which flows a two phase mixture of a liquid and its vapor by summing the contributions of each mechanism by which heat is transferred.

II. THEORY

A. TWO-PHASE PRESSURE DROP

Weekman and Myers [24] published a paper in 1964 in which their experimental data for two-phase pressure drop in packed beds were correlated with theoretical results obtained by them. Their data were compared with those obtained by Larkin, White, and Jeffrey [12] for packed beds and Lockhart and Martinelli [13] for two-phase flow through horizontal pipes. The data by Weekman and Myers fell between the turbulent liquid-turbulent gas and the viscous liquid-turbulent gas curves of Lockhart and Martinelli. This is indeed worthy of notice since the Lockhart-Martinelli data represent two-phase flow through horizontal pipes. This fact prompted the hypothesis that a large number of channels in the porous medium may function in the same manner as pipes in two-phase concurrent flow.

Larkin, White, and Jeffrey also studied experimentally the pressure drop in two-phase flow through packed beds. Their curves were significantly lower than those of Weekman and Myers and those of Lockhart and Martinelli since they corrected their experimental pressure drop results for the mean density in the vertical column. The mean density was defined as:

$$\rho_m = \rho_l S_l + (1-S_l)\rho_g \qquad (2)$$

The mean density defined in this manner is based on the total volume of liquid held up in the bed and neglects the fact that a significant amount of liquid may be supported by the packing due to capillary attraction and may not contribute to the static pressure gradient in the vertical column. Under static conditions for which the static pressure gradient is zero a substantial amount of liquid may be held in a packed bed. Therefore, the static pressure drop in the flowing column may be less than the drop calculated with ρ_m used as the flowing density.

Weekman and Myers, in a paper published in 1964, treated only the two-phase pressure drop across a porous bed through which air and water were flowing downward concurrently. They presented another paper [25] in which the same experimental apparatus and similar flow conditions were used to study heat transfer characteristics. In their second paper, no consideration was given to the two-phase pressure drop.

There is evidence to indicate that the two-phase pressure drop across a porous bed in which a liquid and its vapor is flowing concurrently under non-adiabatic conditions is the same, under certain conditions, as two-phase flow through pipes. In order to demonstrate this, an equation for the two-phase pressure gradient for flow in pipes due to Owens [17] is presented and compared to the experimentally

determined pressure gradient for concurrent two-phase flow of a liquid and its vapor through a porous bed as obtained in the present study. The two-phase flow of a vapor-liquid mixture in a channel with heat addition is a variable density flow and is treated as a one-dimensional flow. If the pressure drop along the channel is relatively small compared with the absolute pressure, the flow of each phase is practically incompressible. The change in bulk flow density is thus due to the phase change caused by boiling. During the process of phase change, or saturation increase, the phase and velocity distributions are changed and so is the momentum of the flow. Owens obtained the total pressure gradient at a point of a vertical two-phase flow by considering three-components, frictional loss, momentum change, and elevation pressure drop arising from the effect of the gravitational force field.

$$\left(\frac{dp}{dl}\right)_{TP} = \left(\frac{dp}{dl}\right)_{f} + \left(\frac{dp}{dl}\right)_{mom} + \left(\frac{dp}{dl}\right)_{elev} \tag{3}$$

where each term of eq. (3) is a function of position. The pressure drop for a given channel length L may be written:

$$\Delta p = \int_{0}^{L} \left(\frac{dp}{dl}\right)_{TP} dl \tag{4}$$

The pressure drop due to elevation depends only upon the local saturation and is not a function of the flow pattern.

$$\left(\frac{dp}{dl}\right)_{elev} = \frac{\rho_m g}{gc} \tag{5}$$

The head loss due to friction for fluid flowing in a pipe is given by the Darcy-Weisbach equation,

$$h_f = \frac{f V^2 L}{2Dg} \tag{6}$$

or

$$\rho g \frac{h_f}{L} = \frac{p_2 - p_1}{L} = \left(\frac{dp}{dl}\right)_f \tag{7}$$

therefore

$$\left(\frac{dp}{dl}\right)_f = \frac{f G^2 v}{2Dg} \tag{8}$$

Owens assumed the friction factor f for single-phase liquid flow to be the same as the two-phase friction factor, f_{TP}. Making this substitution, eq. (8) becomes,

$$\left(\frac{dp}{dl}\right)_f = \frac{f_{TP} G^2 v}{2Dg} \tag{9}$$

Owens [17], Martinelle and Nelson [14], and McAdams, Woods, and Heroman [16] presented results for the two-phase pressure gradient assuming homogeneous flow in which the two-phase friction factor was the same as for single phase flow. Each investigator approached the problem separately and in a different manner and obtained experimental results demonstrating the validity of the assumption.

The pressure gradient due to momentum change may be written:

$$\left(\frac{dp}{dl}\right)_{mom} = \frac{G^2}{g}\left(\frac{dv}{dl}\right) \tag{10}$$

Substituting eqs. (5), (9), (10) into eq. (3) yields,

$$\left(\frac{dp}{dl}\right)_{TP} = \cdot \int_{TP} \frac{G^2 v}{2Dg} + \frac{G^2}{g}\left(\frac{dv}{dl}\right) + \rho_m\left(\frac{g}{g_c}\right) \tag{11}$$

An expression for the two-phase specific volume for homogeneous flow may be written in terms of the quality,

$$v = v_l + \chi(v_g - v_l) \tag{12}$$

The total derivative of v is,

$$\frac{dv}{dl} = \frac{\partial v}{\partial x}\frac{d\chi}{dl} + \frac{\partial v}{\partial v_l}\frac{dv_l}{dl} + \frac{\partial v}{\partial v_g}\frac{dv_l}{dl} \tag{13}$$

Substituting eqs. (12) and (13) into (11), Owens obtains

$$\left(\frac{dp}{dl}\right)_{TP} = \frac{\int_{TP} \frac{G^2 v_l}{2Dg}\left[1 + \chi\left(\frac{v_g}{v_l} - 1\right)\right] + \frac{G^2 v_l}{g}\left(\frac{v_g}{v_l} - 1\right)\frac{d\chi}{dl}}{1 + \chi\frac{dv_g}{dP}\left(\frac{G^2}{g}\right)} \tag{14}$$

$$+ \frac{\frac{g}{v_l[1 + \chi(\frac{v_g}{v_l} - 1)]g_c}}{1 + \chi\left(\frac{dv_g}{dP}\right)\left(\frac{G^2}{g}\right)}$$

Although the test section is vertical the term for pressure drop due to change in elevation was excluded as it was negligible for all runs. Using this expression, Owens predicted the two-phase pressure drop within 30% of the measured pressure drop for flow in a pipe.

In the present study, the pressure drop for two-phase flow through porous media was calculated using eq. (14) and compared to the two-phase pressure drop for flow through pipes as obtained by Owens. The friction factor was calculated using:

$$f_{TP} = \frac{0.316}{(R_e)^{0.25}} \tag{15}$$

$$R_e = \frac{V_1 D}{\nu_1} \tag{16}$$

The pressure dependent terms $v_g - v_1$, and $\frac{dv_g}{dP}$ were calculated from the local pressure with values obtained from Keenan and Keyes [11]. The results will be discussed in a later chapter.

B. EFFECTIVE THERMAL CONDUCTIVITY

It is common practice to treat an elaborate energy transfer device in a qualitative or overall manner without attempting to thoroughly investigate the fundamental mechanisms of transfer within an element large enough to be representative of the whole and small enough to allow a complete understanding of what is happening within. The transfer of heat through porous media is of considerable importance. Therefore it is desirable to formulate a theory to predict the effective conductivity of a heterogeneous system from the conductivities of its constituent parts.

The task of developing a general theory for the transfer of heat through a heterogeneous system is almost impossible. Even in the rather simple case of conduction of heat through a system of spheres packed in a regular way, the mathematical complexities are such that the detailed problem has never been completely solved. On the other hand, where the system consists of granulated material of undefined shape and where the packing is irregular, a direct mathematical solution of the detailed flow and heat transfer in the pores is entirely impossible.

Due to the mathematical difficulties present, no attempt will be made to discuss the general problem of the conduction of heat through a heterogeneous system. Rather, the analysis will be confined to one particular case, which is simpler than the general case and of more practical importance.

The effective thermal conductivity of a porous bed through which a two-phase mixture is flowing can be estimated by considering a simple model for radial heat transfer and assuming that all the various heat transfer mechanisms can be lumped into two terms. The heat transfer associated with the solid particles constitutes one term, while the heat transfer of the two-phase mixture constitutes the other and each term is weighted according to the fraction of the volume it occupies. Since, in the experiments conducted as part of the present study, local temperatures inside the porous bed were low enough so that radiation heat transfer could be neglected. This condition is assumed to apply

in the analysis given herein. Therefore, the principal modes of heat transfer are conduction through the solid phase and transfer by conduction and convection through the two-phase mixture. The assumption is made that the principal heat transfer is radial and is substantiated in the experiments.

Theoretically, the porosity of a packing of uniform spherical particles should be independent of the size of the spheres. However, actual measurements show that for sands (diameters in the range 0.4 mm to 0.25 mm) of essentially uniform grain size, the porosity increases as the grain size decreases [4]. Due to the bridging and wall effects, it is almost impossible to obtain anything approaching a uniform packing by pouring beads into a container as was done when the test channel was filled with 3 mm diameter spherical beads.

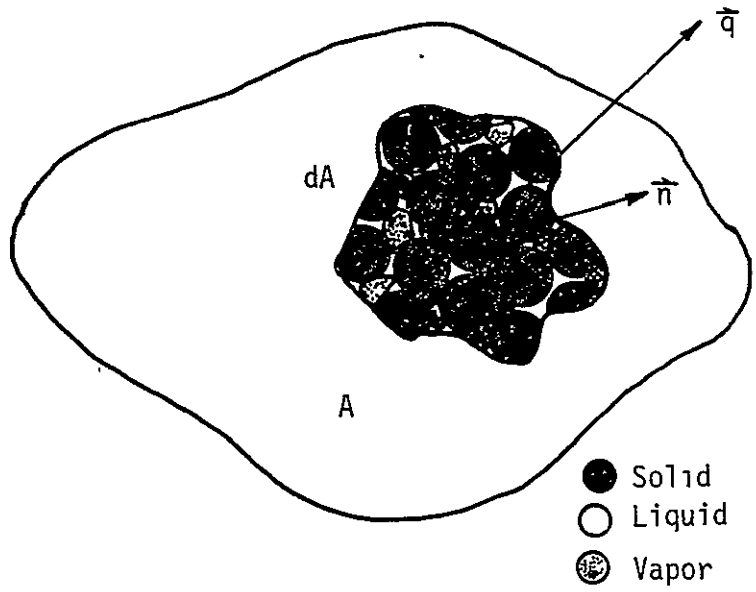

Figure 1. Control Volume of Porous Bed

Figure 1 is an arbitrary control volume of a porous medium enclosed by the surface A through which heat energy is transferred to the surroundings. The modes of heat transfer are conduction and convection, neglecting radiation because of the low temperatures. The total amount of heat transferred by conduction from the control volume can be expressed in terms of the heat flux vector $\vec{q}$ integrated over the surface of the control volume.

$$Q = \oint_A \vec{q} \cdot \vec{n} \, dA, \tag{17}$$

where n is the outward normal unit vector at a point on the surface, and ds is an element of surface area. $\vec{q}$ can be expressed as the product of an effective thermal conductivity of the porous medium and a temperature gradient,

$$\vec{q} = -k\vec{\nabla T} \tag{18}$$

therefore,

$$Q = -\int_A k\vec{\nabla T} \cdot \vec{n} \, dA \tag{19}$$

A portion of the surface area dA is occupied in part by a solid, in part by liquid, and in part by vapor.

The k in equation (18) is the coefficient of heat conduction through the incremental surface area dA of the control volume, which must be general enough to include the effect of each of the following:

1. Thermal conductivity of the solid particles.
2. Thermal conductivity of the liquid.
3. Thermal conductivity of the gas.

Since heat transfer by conduction is proportional to area, the thermal conductivity for the porous medium and two-phase flow will be weighted according to the contribution of each constituent making up the flow field. Equation (19) may be written;

$$Q = -\int_A [k_s(1 - \phi) + \phi k_{TP}] \vec{\nabla T} \cdot \vec{n} \, dA \tag{20}$$

where ϕ is the porosity of the porous bed representing the ratio of fluid volume to total volume as well as the ratio of fluid area to total area (for randomly packed beds). Thus, ϕA represents the fractional part of the control surface area which passes through the fluid and $(1 - \phi)A$ represents the portion which passes through the solid grains. k_s is the thermal conductivity of the solid particles and k_{TP} that of the two-phase mixture.

Since, the resistance to heat transfer by conduction of the two-phase mixture may be separated into that due to the liquid and that due to the vapor, the following may be written:

$$k_{TP} = Sk_v + (1 - S)k_l \tag{21}$$

where S is the ratio of vapor volume to total volume of void space (S also represents ratio of areas when the bubble distribution is random), where k_v and k_l are the thermal conductivities of the vapor and liquid, respectively. Hence the total heat conduction can be written as:

$$Q = -\int_A [(1 - \phi)k_s + \phi S k_v + \phi(1 - S)k_l]\vec{\nabla T}\cdot\vec{n}\, dA \qquad (22)$$

or

$$Q = -\int_A K_c \vec{\nabla T}\cdot\vec{n}\, dA \qquad (23)$$

where

$$K_c = (1 - \phi)k_s + \phi S k_v + \phi(1 - S)k_l \qquad (24)$$

K_c is defined as the effective heat transfer coefficient due to conduction which consists of the sum of the contribution of each constituent making up the flow field. The thermal conductivities of the solid, liquid, and vapor are taken from references [6] and [9]. These conductivities vary only slightly over the temperature range in which tests were conducted and are taken at the average of the centerline temperature of the porous bed and channel wall temperature.

In the present experiments the direction of principal heat transfer was radial or perpendicular to the centerline of the channel, therefore, the discussion of heat transfer coefficient is specialized to apply to the radial direction only. The total effective radial thermal conductivity

at a particular cross-section may be written as:

$$K_e = K_c + \phi K_R \tag{25}$$

where K_r is the contribution to the overall effective thermal conductivity of the radial movement of liquid and vapor caused by the tortuous channels in the randomly packed medium. It is emphasized that, because none of the small random channels are straight, radial velocities exist at any cross section even though the net radial flow is zero. K_e was calculated experimentally at five locations where there were meters for determining the saturation.

If K_R is a constant in a cross section, at any cross section in the porous bed, the average heat flux per unit area through the walls of the channel that is caused by convection may be expressed as the product of K_R and the temperature difference between centerline and wall. This flux may also be written directly in terms of the convection phenomenon. Therefore when these two expressions are equated the following results:

$$K_R \frac{T_w - T_{\ell}}{L} = \gamma V_0 \rho_l C_{Pl} (T_w - T_{\ell}) + \beta V_0 \rho_v C_{Pv} (T_w - T_{\ell}) \tag{26}$$

in which V_0 is the flow rate of the liquid divided by the total area of the channel. β is the radial fraction of the liquid velocity, γ the radial fraction of the gas velocity, L the distance from the centerline of the porous bed to the inside channel wall, T_w the inside channel wall temperature,

and T_{ℓ} the centerline temperature of the porous bed. Therefore, $\gamma V_0 \rho_l$ is that portion of the total mass velocity having a component in the radial direction. It is the consensus of earlier investigators [7][24] that the presence of vapor flow in the radial direction only increases the magnitude of the liquid velocity and has no bearing on the amount of the total mass velocity having a radial component which has been accounted for by introducing γ. Investigation of the relative magnitude of each term on the right side of equation (26) reveals that the only term with appreciable magnitude is the term accounting for the heat flux convected radially by the liquid [7], thus eq. (26) becomes:

$$K_R = \gamma V_0 \rho_L C_{PL} L \tag{27}$$

In the experiments conducted for this study, the liquid mass flowrate was measured before the liquid entered the test channel, therefore V_0 is determined by applying the equation of continuity. γ is taken to be 0.00174 from the works of Golpalarathnam, Hoelscher, and Laddha [7], and Weekman and Myers [24]. Both observed that the amount of heat transferred did not appear to be a function of particle size.

The equation for predicting the effective thermal conductivity of a porous bed in which concurrently flows a two-phase mixture of a liquid and its vapor is submitted to be of the form:

$$K_e = (1 - \phi)k_s + [Sk_v + (1 - S)k_l] + \gamma V_0 \rho_l C_{Pl} L \phi \quad (28)$$

With the effective thermal conductivity presented in this form, the contribution of each constituent can be investigated.

III. DESCRIPTION OF EXPERIMENTAL APPARATUS AND SUPPORTING EXPERIMENTS

A. TEST CHANNEL

The aluminum channel (Figure 2) housing the porous bed, saturation meters, pressure transducers, inlet heater and thermocouples was 24 inches long with inside dimensions 2 inches by 3 inches with plates fastened at both ends. The entrance end plate contained a heating element and access posts for electrical connections to the heater. The channel was constructed by cutting and welding together two 4 inch by 4 inch by 1/4 inch angles. The 1/8 inch radius fillet at the base of each angle was machined out to make all corners square.

On each 3 inch side of the channel were two viewing windows 2 inches by 8 inches by 1/4 inch made of Pyrex glass attached to the channel within a slot, 2 1/16 inch by 8 1/16 inch. The clearance between wall and glass was filled with RTV-106 silicone rubber sealant. To keep the glass from being pushed out due to internal pressure, a slotted plate with gasket was fastened over the glass on the outside of the channel. Care was taken to prevent metal to glass contact to lessen the danger of breaking. Five

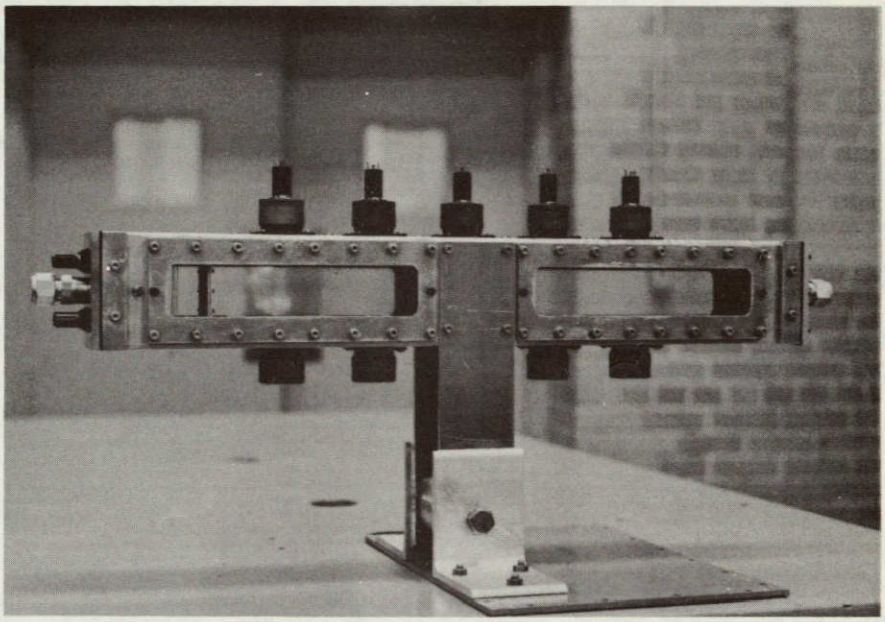

Figure 2. Aluminum Channel

circular windows were placed 3 inches between centerlines opposite each other on each of the 2 inch sides such that light from one window could be transmitted through the bed to a photodiode on the opposite window. These windows were made of 1 inch diameter Pyrex glass 1/8 inch thick placed in a 1 1/8 inch diameter hole flush with the inside wall. The clearance space between the window and hole was filled with sealant.

Pressures were measured by four Consolidated Electrodynamics Corporation (CEC) transducers placed along the center of one of the 2 inch walls. The first was placed 7 1/2 inches from the inlet and the others 3 inches between centerlines midway between the photodiodes. The transducers were 1/2 inch diameter with flush mounted diaphragm and fitted into a counterbored hole on the outside wall of the channel. They were held securely by a collar which slid over the transducer and bolted to the channel wall. The counterbored hole was connected to the inside of the channel by seven holes (0.0135 inches in diameter) which were drilled perpendicular to the channel center line and spaced equally across the 1/2 inch diameter hole. This allowed the pressure transducer to experience changes in fluid pressure and not be in contact with the glass beads.

Temperatures along the channel centerline were measured by seven thermocouples, the leads to which were inserted through a hole in a 5/16 inch diameter bolt sealed by epoxy. The bolts were screwed into holes in the wall such

that they were flush with the inside wall. The first thermocouple was placed 4 1/2 inches from the inlet and the others on 3 inch centerlines between the lights.

All temperatures were measured by thermocouples made from copper-constantan wires. The centerline temperatures of the porous bed were measured by thermocouple junctions soldered into a copper spheres the same diameter as the glass beads. The sphere and wires were insulated by lacquer spray. The inside wall temperature of the channel was measured by drilling a small hole in the wall and pressing a copper slug which contained a thermocouple junction into the hole. The temperature of the liquid in the accumulator tank was measured by an insulated thermocouple junction.

The saturation meters each consisted of a 28 volt dc light source and photodiode biased by a 0-40 volt dc power supply with its output measured on a microammeter in series with the power supply. The light source was placed on one 2 inch side of the channel behind a 1 inch diameter glass window. The photodiode was placed on the opposite side behind a 1 inch glass window. The center of the first meter was placed six inches from the channel inlet and the other four on three inch centerlines.

The end plate (Figure 3) through which the fluid entered the porous bed supported a teflon frame for the heater wires, electrical connections, screen, and baffle. The heater which extended 2 1/2 inches into the porous bed

was made of 24 B. and S. gage (0.0201 inch diameter) 1.478 ohms per foot Chromax Alloy wire (Driver-Harris Company) wound around two strips of teflon. Since the wires were uninsulated, extreme care was taken to maintain a space between adjacent wires. Two insulated electrical feed-throughs were placed in epoxy sealed drilled holes in the end plate soldered to a 1/8 inch diameter copper bus bar which was connected to the heater wire. On the inside surface of the end plate a screen was mounted to hold the beads and an aluminum plate 3/4 inch by 1 1/4 inch by 1/16 inch with 3/16 inch diameter holes was attached 1/2 inch from the screen to break up the bulk of entering fluid. The exit end was closed by a plate which had a screen over the opening. The entire channel was attached to a 1/4 inch aluminum base plate which was bolted to a table. A hinge arrangement allowed the channel to be rotated 90° from the vertical.

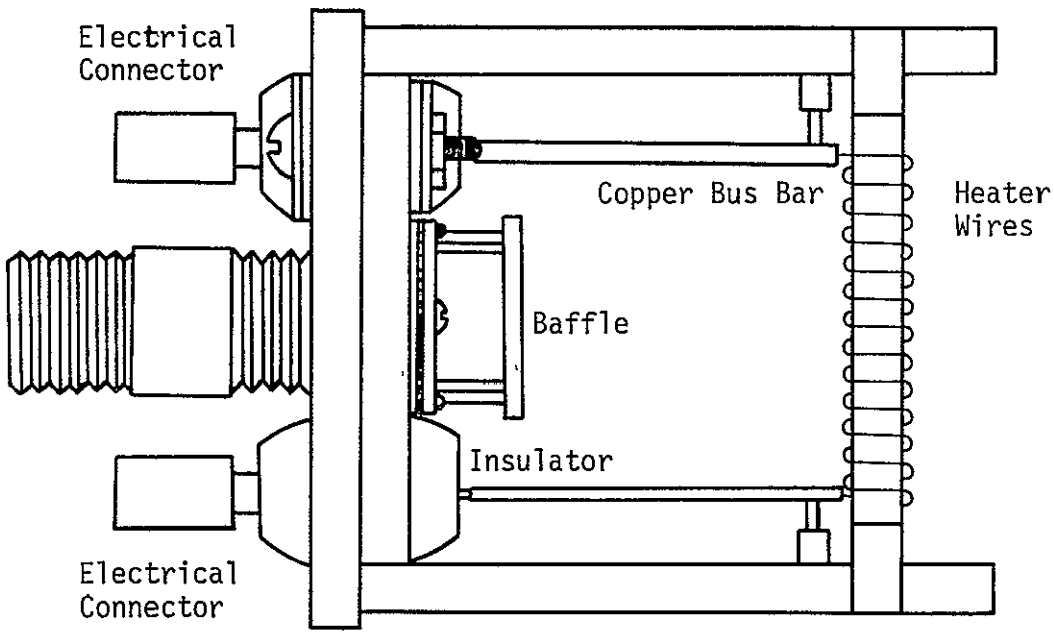

Figure 3. End Plate

B. FLOW CIRCUIT

Shown in Figure 4 is a diagram of the flow circuit. Fluid was pumped from a 14 gallon tank through type 304 stainless steel tubing (0.402 inch I.D. and 0.049 inch wall thickness) using brass Swagelok connectors. The stainless steel tank was 12 inches in diameter, 30 inches high and 1/4 inch wall thickness closed by a gasketed lid forming a pressurized accumulator chamber. Band heaters were placed around the tank to heat the liquid before a test began. Installed in the lid were a pressure gage and a back pressure relief valve. Thermocouple leads passed through the lid to a junction within the liquid.

A Viking Model FH-54G pump was used downstream of the tank. Inserted in the line between the tank and pump was a bronze valve and filter made of small mesh copper screen. The pump was constructed of all bronze parts with a mechanical seal and bronze relief valve. It was capable of pumping a maximum of 3 gallons per minute at 25 psi. discharge pressure and was driven through a flexible coupling by a 1/3 horsepower variable speed direct current motor with speed range between 0 and 1800 rpm.

Downstream of the pump, the liquid flowed thru a Pottermeter flow sensing element incorporating a high efficiency rotor which spun freely within a venturi. This unit was capable of withstanding temperatures in a range from -456 °F to 1000 °F and pressure up to 5000 psi. The element

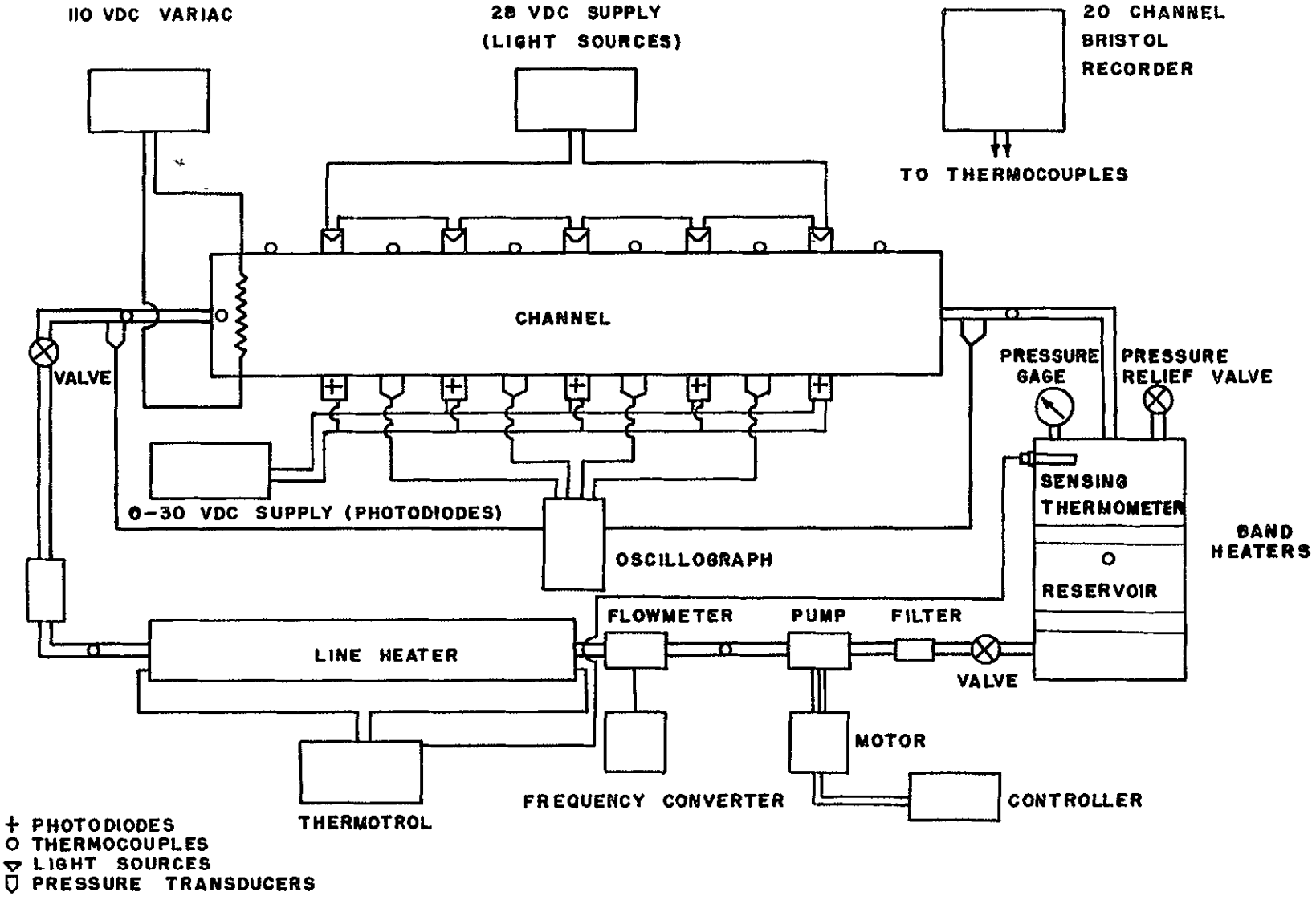

Figure 4. Flow Circuit

consisted of a housing designed to adapt directly into the piping in which a hydraulically self-positioned rotor was suspended. As the fluid flowed through the element, the rotor revolved at a speed determined by the velocity of the fluid. Mounted on the outside of the housing was a pick-up coil, so placed that the rotation of a magnet created an AC voltage of frequency equal to the speed of the rotor. Since the sensing element was a frequency device, only flow factors which affect the rotating speed of the rotor could influence the flowmeter accuracy. Therefore, fluid viscosity, pressure, temperature, and specific gravity have only slight effects on the volumetric flow rate. The output signal from the sensing element was fed into a Model 3C-N Electronic Frequency Converter. The Potter-meter and frequency converter assembly was calibrated using a suspended float rotameter (Figure 5).

After passing through the pump, the liquid was heated by a 1000 watt immersion heater silver brazed into the 1 inch O.D. copper tube located upstream of the entrance to the channel. The power input to the heater was controlled by a Model 1053 Thermotrol Temperature Controller designed to operate by any one of three different modes: On-off, Proportional, or Proportional with Reset. In these experiments it was operated in the On-off mode.

Out of the immersion heater the water flowed through a filter, into the channel, and back into the tank.

Figure 5. Calibration Curve For Potter Electronic Frequency Converter

C. EXPERIMENTAL PROCEDURE

As previously mentioned, the purpose of this experiment was to study boiling flow through a porous medium. In order to treat this phenomenon, an experimental apparatus was constructed and used for the experiments described herein. For a particular flowrate, values of saturation, pressure, and temperatures were measured in the flow field. The procedure for conducting a typical experiment will be described.

To begin a test, the 14 gallon accumulator chamber was filled with distilled water and the water pumped around the flow circuit. The band heaters around the accumulator chamber and the in-line heater heated the water to a few degrees below saturation temperature which was about 218 °F. It required approximately two hours to heat this amount of water. At this temperature the band heaters and in-line heater were manually turned off and power was applied to the heater in the channel producing boiling. The voltage applied to the heater in the channel was adjusted to a predetermined value by means of an alternating current variac.

Saturation was determined by using a previously calibrated meter consisting of a light source and photodiode. For a constant intensity light ray received by a photodiode, its output is a function of the bias voltage and for identical bias voltages the output is different for each photodiode.

When calibrating the meters each photodiode was biased to produce an output of 12 μa at zero gas saturation i.e., with clear liquid flowing through the channel. This particular voltage was called the calibration bias and was different for each photodiode. When gas saturation was measured the calibration bias voltage was applied to the photodiode and the corresponding output read from the microammeter. When one saturation meter was being read, all the other lights were off to prevent light interference affecting this meter. Also the Pyrex windows on the channel were shielded to prevent outside light from affecting the photodiode output. Because each of the meters was powered by the same power supply, the calibration bias voltage had to be reset on each meter before saturation could be measured.

Each time the saturation in the channel was measured, a permanent pressure-time trace was taken. This trace was obtained by applying 5 volts dc excitation voltage to each transducer and feeding the output current into a Model 1508 Honeywell Visicorder Oscillograph Recorder. The deflection of the Visicorder output trace was calibrated against the existing pressure in the channel. This will be discussed in a later section. Before a test began, a calibration trace for each transducer was obtained at room conditions and the power supply to the Visicorder was kept on for the duration of a test. When a pressure trace was desired, the run button on the Visicorder was punched and

a short segment of paper obtained which contained the pressure trace.

A precision pressure gage, installed in the lid of the accumulator tank, indicated the pressure of the vapor above the water surface in the tank. A pilot relief valve was set to maintain this pressure at a constant value. This pressure served as a datum to indicate the system pressure.

Temperatures at several points in the flow circuit were monitored from the beginning to the end of a series of tests. Each of the pairs of wires leading from a thermocouple was fastened to a Bristol Temperature Recorder which stamped a numbered dot on the chart paper. This paper was continuously advancing at a constant rate and had grid lines marked in degrees Fahrenheit; therefore the temperature at any particular location could be read from the chart. This also provided a permanent temperature record for the duration of a test. It was necessary to calibrate the recorder at the freezing point and boiling point of water.

A test series is defined as a group of tests each having the same voltage (hence power) applied to the channel heater. Tests series were run for channel heater voltages 40, 45, and 50 volts. For each series liquid water flowrate was initially set at 0.48 gpm. Complete data were recorded for this flowrate and 5 additional flowrates at increments of 0.48 gpm with a maximum of 2.88 gpm.

D. CALIBRATION

Saturation Meters

The saturation meters were calibrated in a special channel constructed specifically for calibration purposes. This channel had the same cross-sectional dimensions as the experimental channel and was 12 inches long. The meter was placed near the exit so that the injector disturbances would not affect the calibration. In the calibration setup weight decrement was used as a measure of total gas volume within the channel, and thus an indication of average saturation. In order for the average saturation to be the same as that in the cross section of the meter, nitrogen was injected into the channel as the gaseous phase. This eliminated the problem of vapor condensation in the interior of the channel. Such condensation would mean that the average saturation would be different from that measured at the meter cross section. The indices of refraction of nitrogen gas and water vapor are almost identical. Thus the calibration obtained in this manner was applied to the meters when used in the boiling experiments.

The light passing through the bed was detected by the photodiode placed directly across the channel from the light. The intensity of the light detected by the photodiode was dependent upon the absorption and dispersion of the light rays by the solid particles and different interfaces

within the porous bed and was indicated by the current output of the photodiode. The light was dispersed by striking an interface formed by two different mediums. With clear water flowing through the porous bed, the number of interfaces dispersing the light was a minimum. The introduction of bubbles in the fluid stream produced additional interfaces (solid-vapor and liquid-vapor). Therefore the amount of gas present governed the amount of light received by a photodiode, and consequently its current output. In order for this to be meaningful, each meter was calibrated for current versus volumetric saturation.

Shown in Figure 6 is the calibration set-up. The volumetric saturation was calculated by weight decrement and the current output of each photodiode corresponding to a particular saturation was recorded. A photodiode is a very sensitive device, therefore to exclude any error from stray light, the inside of the calibration channel and experimental channel was painted with a high temperature aluminum paint. When taking readings on the experimental channel, the glass windows were shielded.

In the calibration circuit water was pumped through 3/4 inch inside diameter flexible clear vinyl tubing. At the point of attachment to the channel, these lines exhibited a certain degree of rigidity, which produced an error in the weight readings. In order to determine this error, known weights were placed on the channel and the corresponding

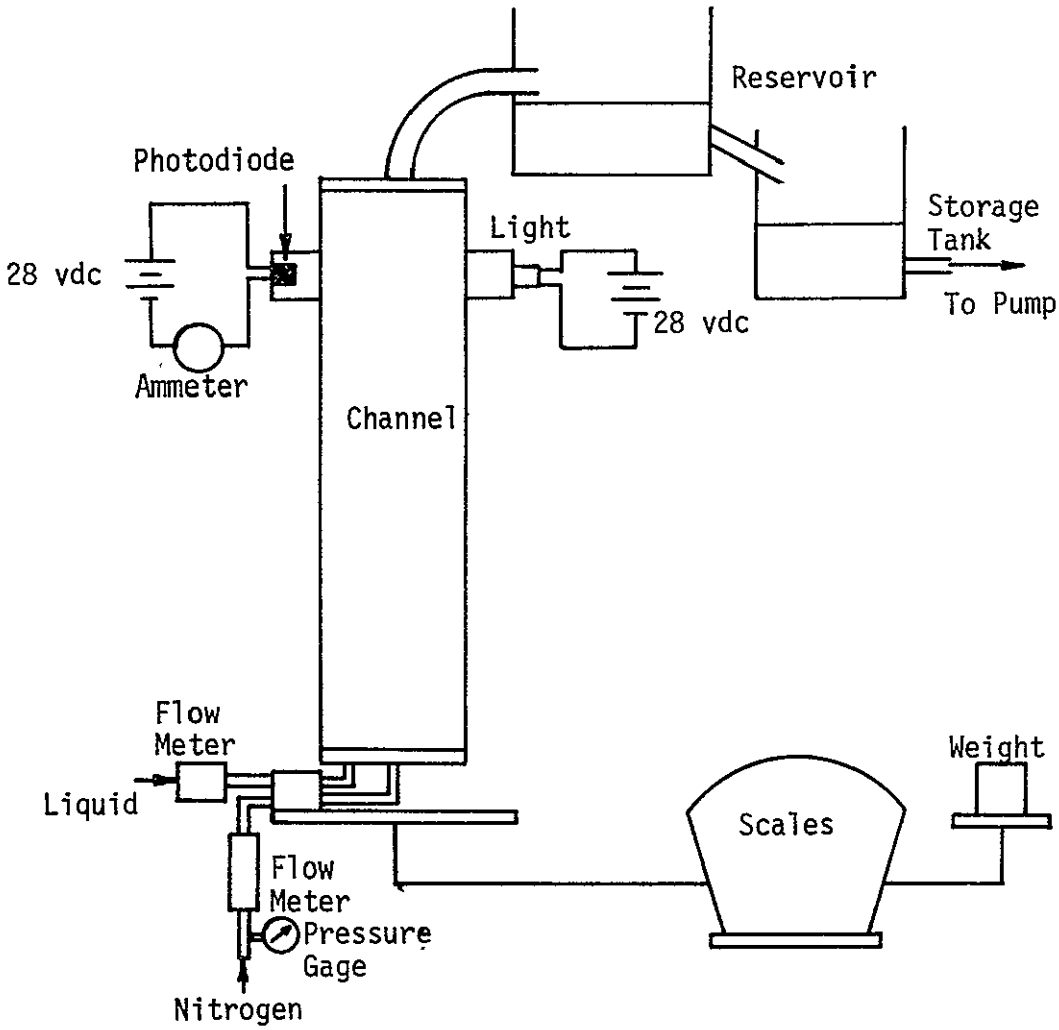

Figure 6. Experimental Apparatus for Calibrating Photodiodes

weight indicated by the scales was recorded. Additional weights were added such that a correction for each indicator position could be determined (Figure 7).

There was also an error due to the momentum change of the liquid at the entrance and exit to the channel. This error varied with water flowrate. To compensate for this, the scales were set at the same initial indicator position each time the flowrate was changed.

The saturation exisiting in the channel was determined by a change in weight indicated by a change of scale position. For clear water flow there was 0.1278 lb of water in the exit line which had to be subtracted from the indicator reading to give the true weight of water in the channel. Upon introducing nitrogen there was also two-phase flow in the exit line. An approximation was made of the weight of water and nitrogen present in the exit line for each saturation. As the saturation was increased the volume of nitrogen in the exit line increased and less correction was required.

In the initial tests, the photodiode output, for zero saturation was different at the beginning and end of a test. Also there was a large fluctuation in the current at each saturation, frequently as much as 2 μa. It was found that this fluctuation was more pronounced at low liquid and gas flow rates and it was decided that this was the result of the bed becoming fluidized at low liquid

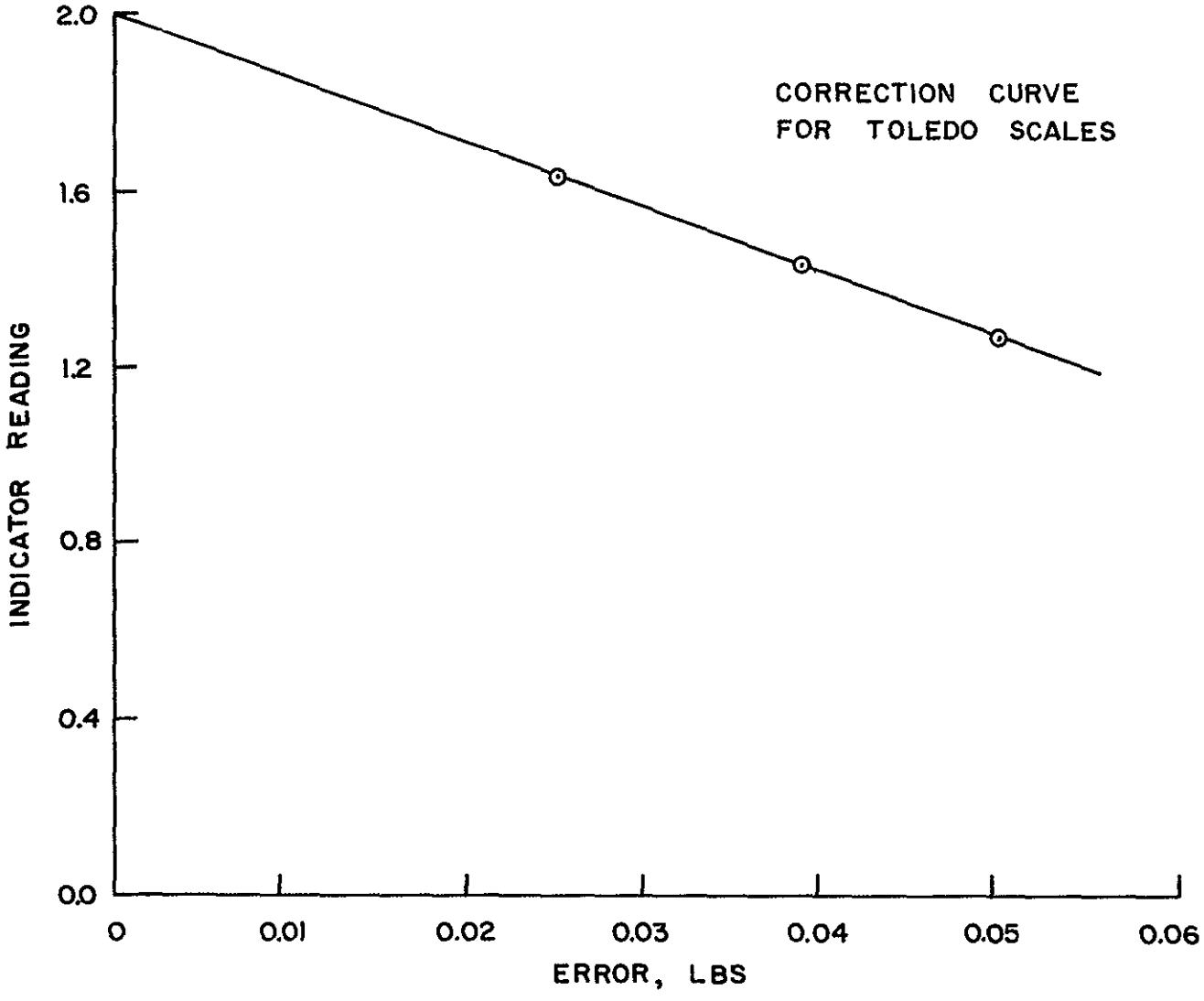

Figure 7. Correction Curve For Toledo Scales

rates. Upon increasing the liquid flowrate, the entire porous bed was at first fluidized and then raised inside the channel. This moving of the bed caused some fluctuation at each indicator position. To solve this problem the bed was packed 10 different times and 2800 beads were added after the initial packing. The most efficient method of packing the bed was to maintain the liquid flowrate constant at 0.96 gpm and pulsate the gas flow through the bed. After these packings the bed stabilized as did the scale readings and the photodiode output was more steady, varying only 0.2 μa at the most.

As was mentioned previously, the channel for the present study was constructed with 5 meters, each meter requiring one photodiode. In Figure 8 the output of each photodiode is plotted against voltage applied to the light source. The variation in impressed voltage is an indication of the light-intensity passing through the porous bed. The same light bulb was always used for a particular photodiode to eliminate any error caused by the variation of intensity of different light bulbs at the same applied voltage. From these curves it is apparent that each photodiode must be calibrated separately. In an attempt to shift these curves such that only one calibration would be required, a variable resistor was placed in series with each photodiode. By applying the same bias voltage to each photodiode, the output could be adjusted by increasing

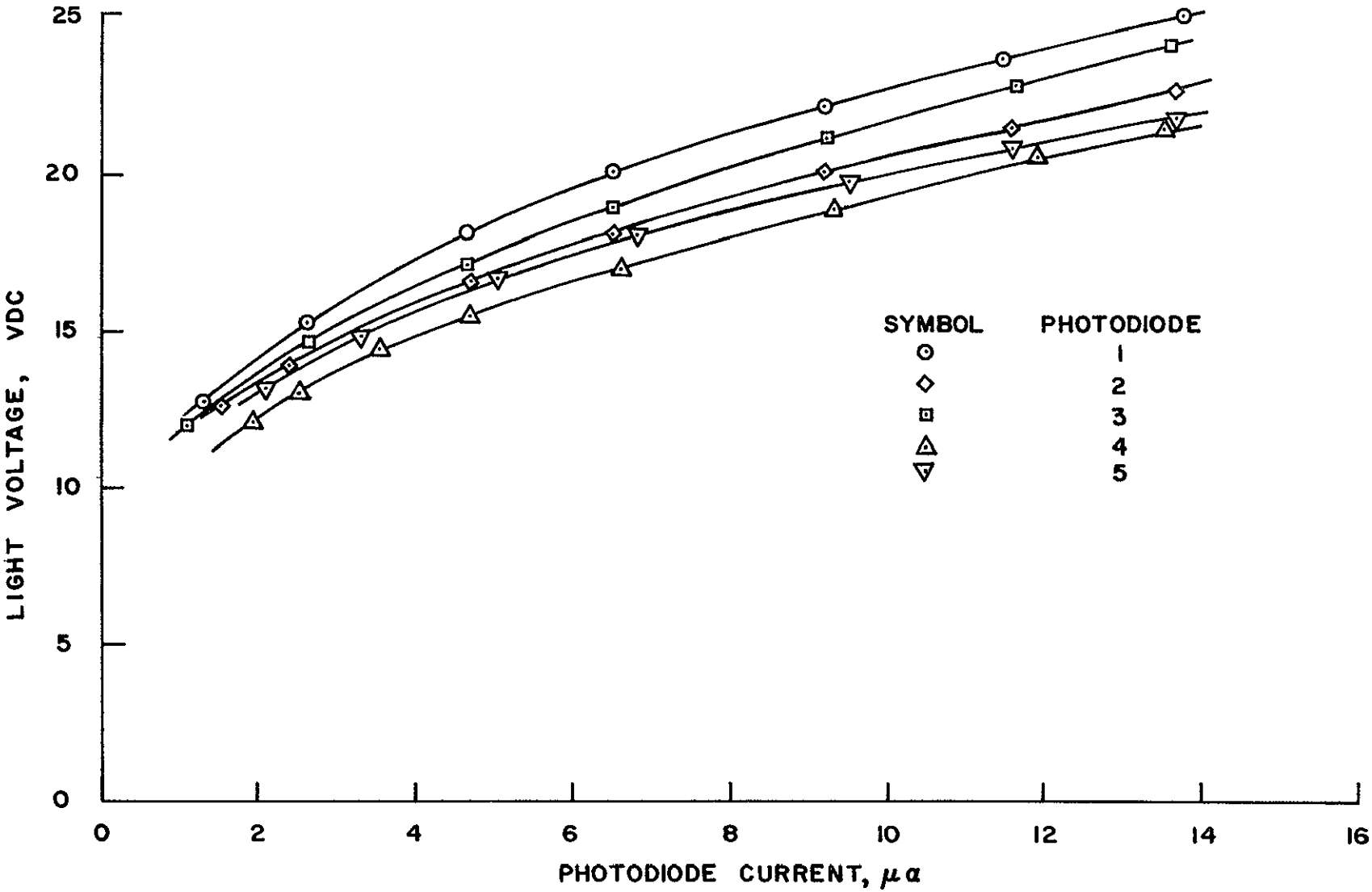

Figure 8. Photodiode Output Versus Applied Light Voltage

or decreasing the series resistor. With the maximum intensity light passing through the bed, the resistance of a photodiode is in the range of 2 meg ohms. This required a series resistor of the same magnitude. However, it was found that due to the large resistance of the series resistor, the voltage drop across this resistor varied as the current output of the photodiode causing an additional fluctuation in the bias voltage. Since each photodiode has a different characteristic curve, then each will have its own calibration curve.

Several different type light sources were investigated. One made by Texas Instruments Corporation which produced light in the infrared spectrum was considered. This source produced a narrow beam with a 20 degree central angle of spread. This type of light source exhibits a change in wavelength with temperature. This characteristic is undesirable for the purpose of measuring light transmission in a flow channel where temperature will be varying. The fact that this light produced a narrow beam was at first thought to be beneficial since a photodiode is directionally sensitive. However, at low liquid and gas flow-rates, or low saturations, the gas bubbles flow through the porous bed along random paths at different frequencies, and the size of the bubbles is larger than for higher saturations. The narrow beam light did not cover enough of the bed to give a true indication of saturation under such

conditions. Therefore, the light source used, namely, a small 28 volt dc bulb requiring 0.17 amps was one which produced a beam covering a large area giving an average of the saturation in the neighborhood of a particular cross section.

The size of the bubbles passing through the porous bed varied with liquid and gas flowrates. At low liquid flowrates, the bubbles were estimated to range from 1/16 inch to 1/4 inch in diameter. As the liquid flowrate was increased, the bubbles were broken up and the number of small bubbles at any one section increased. At high liquid flowrates it was necessary to increase the gas flow to produce the same saturation as at low flowrates. However, it is recalled that the same volume percentage of gas is present for equal saturations. The size of the bubbles influences the amount of light transmitted through the bed and hence the output of the photodiode. Therefore, the fact that the amount of gas at any one section was the same for equal saturations but at higher liquid flowrates the bubbles were smaller in size and produced additional interfaces required calibration for each liquid flowrate. This means that the output of a photodiode at the same saturation will be less at high liquid flowrates than at low flowrates.

When calibrating each saturation meter, nitrogen was used as the gaseous phase and water as the liquid phase.

In the vapor bubble experiment, the gaseous phase was produced by locally boiling the liquid at the entrance to the channel. Since the meter measures the amount of light transmitted through the bed at a particular cross-section, how then, if any, will the different types of interfaces, water and nitrogen, or water and water vapor, affect the calibration? The fact that nitrogen was used will not affect the calibration in so far as the refracted light ray is concerned. In order to verify this, consider Snell's Law of Refraction. When light falls upon an interface separating two different mediums, part is reflected, part is absorbed, and part is refracted into the medium. The angle of refraction depends upon the angle of the incident ray and the index of refraction of the medium through which the refracted ray is passing. Figure 9 shows the two different interfaces. For the same angle of incidence, what is the difference in the angle of refraction?

Snell's Law states that the index of refraction μ in the medium through which the refracted ray is passing is the ratio of the sine of the incident angle i to the sine of the refracted angle r.

$$\mu = \frac{\sin i}{\sin r} \tag{29}$$

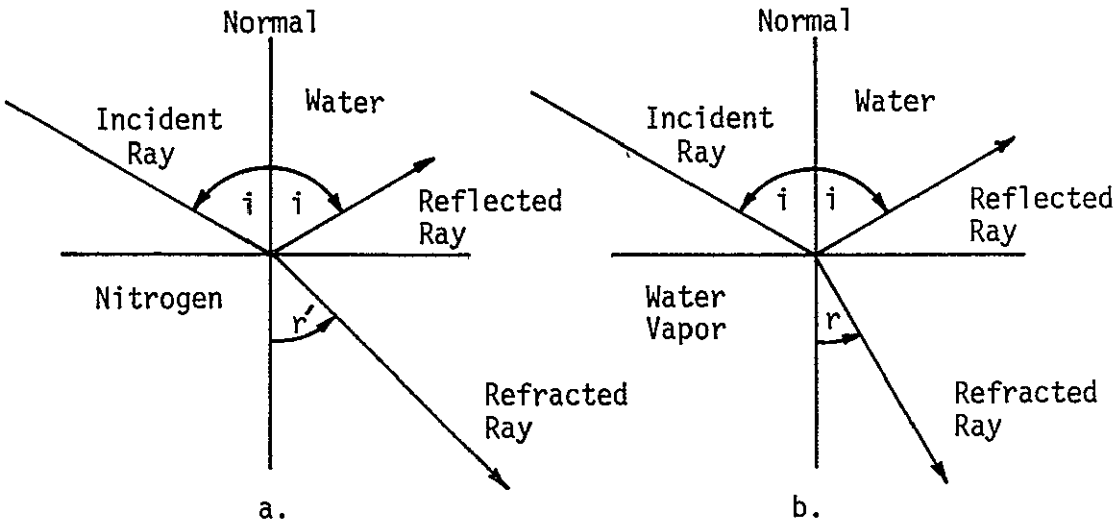

Figure 9. Refraction of a Light Ray Across Two Different Interfaces

For an equal angle of incidence the sine of the refracted angle for the two interfaces is inversely proportional to the index of refraction of the different medium.

$$\sin r = \frac{\sin i}{\mu} \tag{30}$$

$$\sin r' = \frac{\sin i}{\mu}$$

where the prime denotes properties pertaining to nitrogen. Therefore, the angle of refraction varies as the index of refraction for the two gases. The index of refraction for water vapor is 1.000261 and for nitrogen is 1.000296. The difference of 0.000035 is considered small enough such that the calibration will not be affected by using nitrogen as the gaseous phase.

In the vapor bubble experiment where the gaseous phase was produced by boiling the water, the system operates at temperatures higher than room temperature. When calibrating the photodiodes the system temperature was 77 °F. Several tests were run in which the liquid was heated to 120 °F, and this temperature increase had no affect on the calibration curves. Therefore, the calibration does not appear to be temperature dependent.

In Figure 10 is shown the calibration curves for one photodiode at four different flowrates. Each of the five photodiodes have a different set of calibration curves.

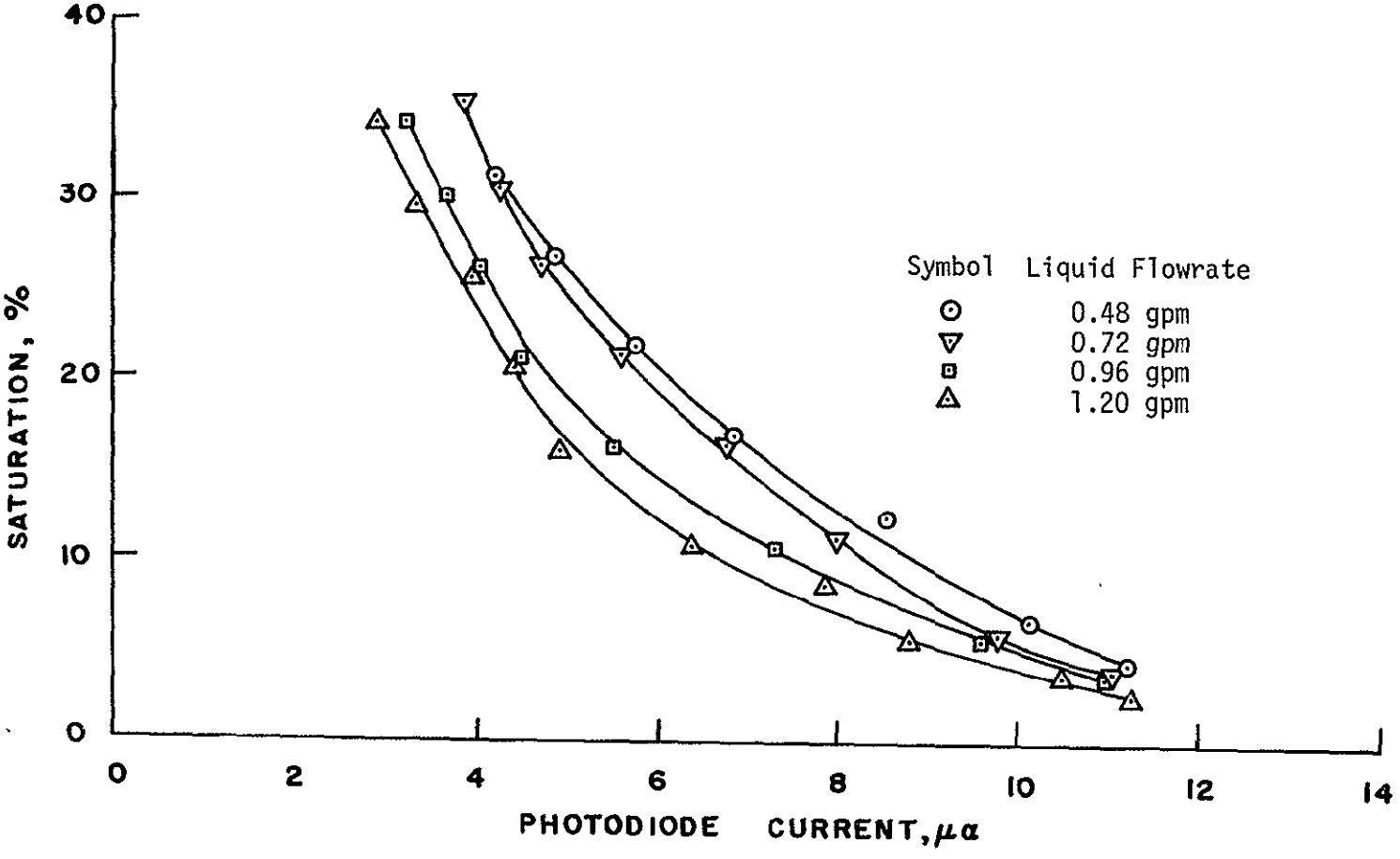

Figure 10. Calibration Curve for One Photodiode

Pressure Transducers

Pressures on the inside channel wall were measured using Consolidated Electrodynamics Corporation (CEC) pressure transducers requiring 5 volts dc excitation voltage. This voltage was supplied by a Model 801C Harrison Laboratory power supply. The transducer output signal was fed directly into a Model 1508 Honeywell Visicorder Oscillograph Recorder which provided a permanent pressure-time curve. For the pressure trace to be meaningful, the Visicorder output signal was calibrated against the corresponding pressure experienced by the transducer (Figure 11).

Six transducers were placed in the flow circuit, one at the channel entrance, four on the channel, and one at the channel exit each requiring a separate calibration curve because of different pressure ranges and internal resistance. This was accomplished by attaching opposite each transducer a pressure tap which connected to an Ametek precision pressure gage. With the inside of the channel open to atmospheric pressure and the gages zeroed, an initial pressure trace was recorded on the Visicorder. Water was then pumped through the channel and at a selected pressure the Visicorder Oscillograph was started and a short segment of paper obtained which contained the deflection from the initial setting representing the particular pressure experienced by the transducer. The pressure required for this deflection was read from the pressure gage and a calibration curve obtained (Figure 12).

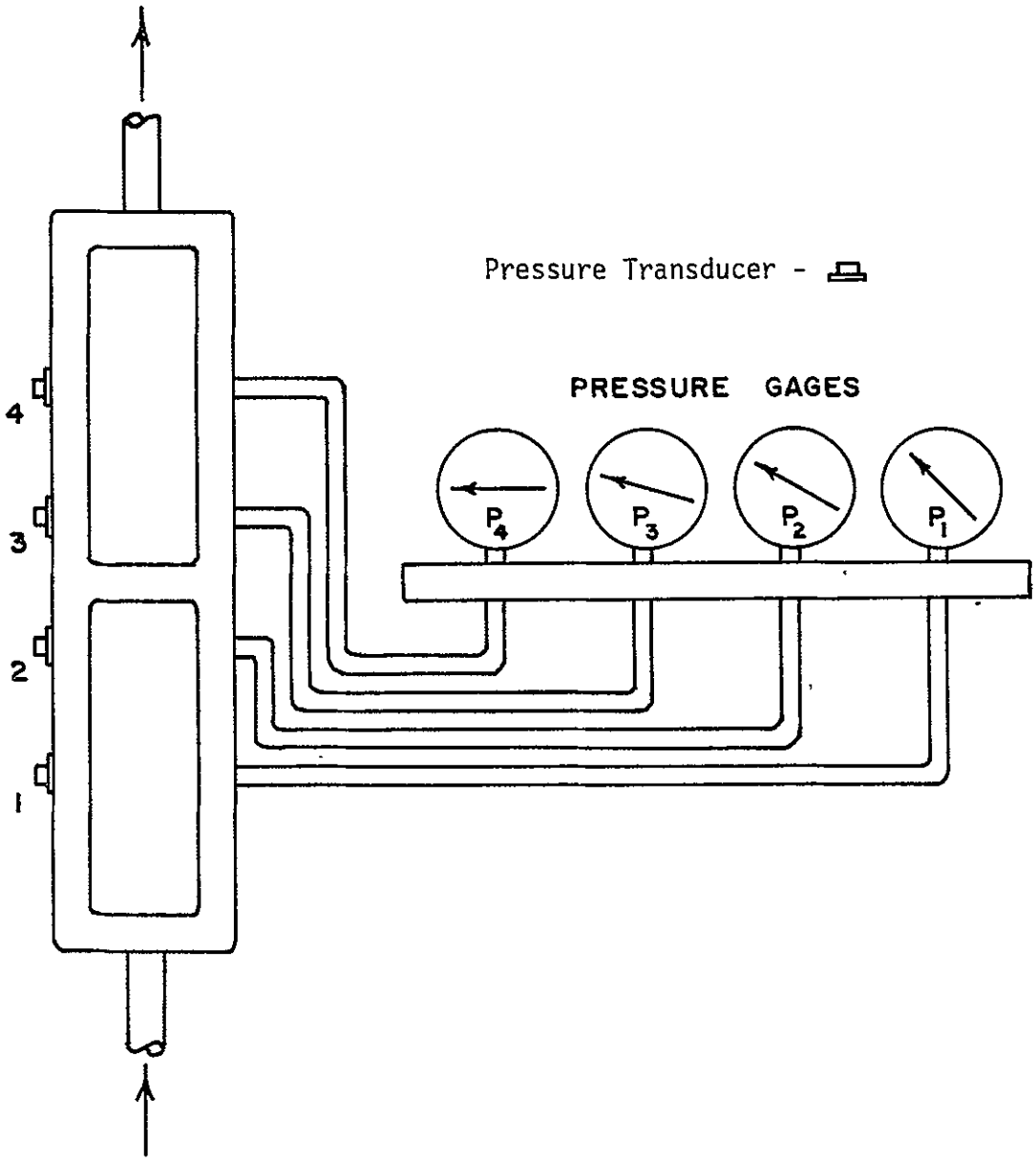

Figure 11. Apparatus for Calibrating Pressure Transducer

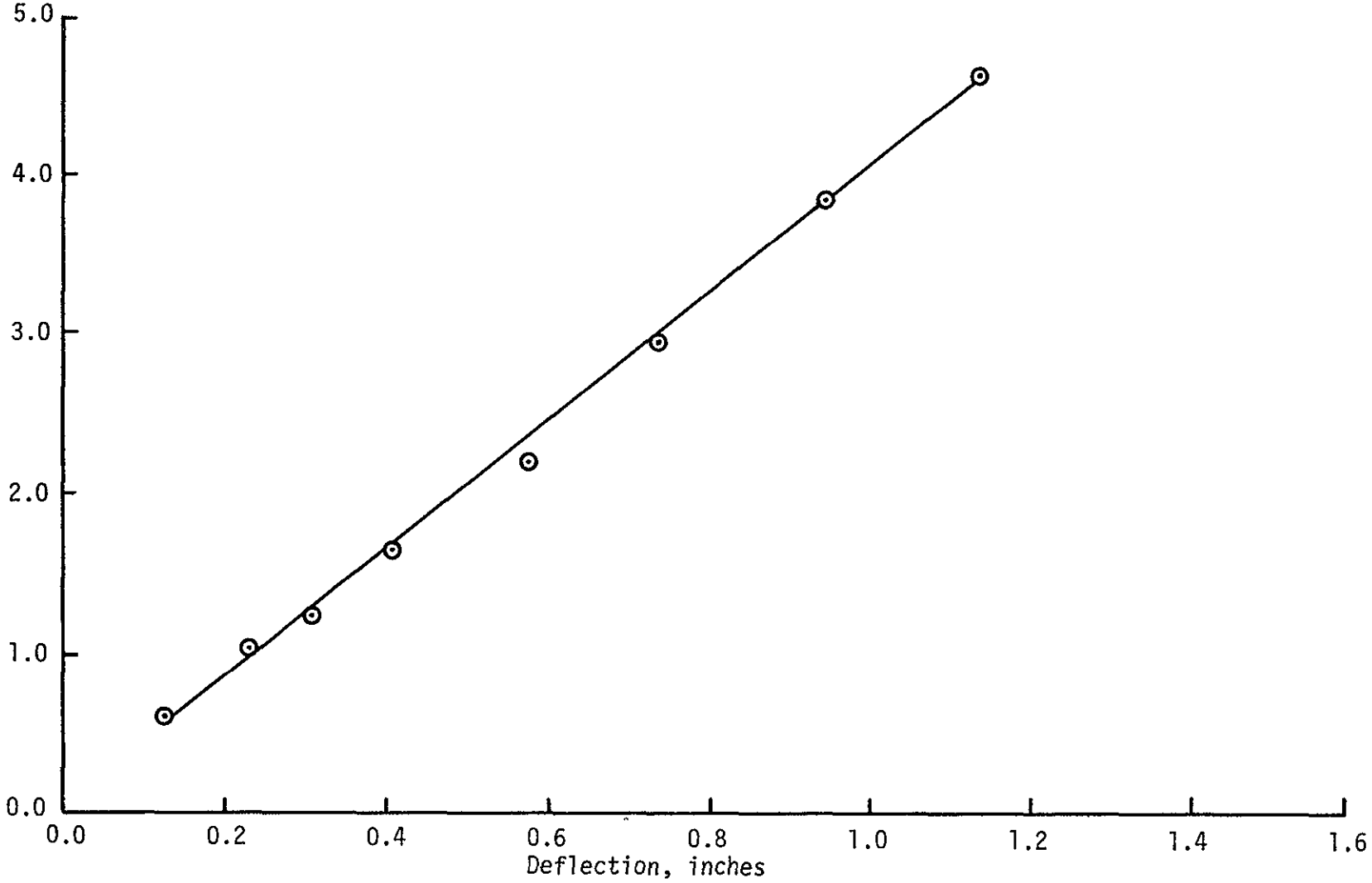

Figure 12. Pressure Tranducer Calibration Curve

IV. EXPERIMENTAL RESULTS AND CONCLUSIONS

The test channel was instrumented such that values of temperature, pressure, and saturation could be measured continuously over a period of time.

In the initial series of tests, the flow of vapor bubbles at a particular flowrate could be observed to some extent through the Pyrex glass windows although no effort was put forth to produce a transparent bed. Since the heater extended into the porous bed the diameter of the bubbles emerging from the heater wire surface was a function of the pore size which was approximately equal to the diameter of the glass beads (3 mm). Visual observations indicated that the vapor bubbles produced by the heater seemed to be of constant size and distributed equally across the cross-section for a distance of 2 or 3 inches above the heater. From this point until the bubbles reached the channel exit, there existed a region along the centerline of the porous bed in which a vapor bubble could travel the entire length of the channel without condensing. As the channel wall was approached in the radial direction at any chosen cross section, the amount of vapor bubbles decreased such that there was almost no flow of vapor adjacent to the inside of the wall.

The saturation changed along the length of the porous bed from the heater to the exit. When the Pyrex observation windows were used there were high values at the heater wires, at mid length and at the exit. Low values existed in the sections containing the two Pyrex glass windows. An approximate explanation of this variation in saturation can be given in terms of longitudinal heat conduction through the channel walls. This conduction occurs from the heat source in the vicinity of the channel heater. Heat flows longitudinally in the channel wall, and this longitudinal heat flow contributes to the total inside wall temperature. The glass windows are much better insulators than the aluminum wall; therefore the temperature of the glass window would not be raised as much as the walls due to longitudinal conduction. Therefore condensation would be greater adjacent to the glass windows than in the cross-sections surrounded by aluminum walls. Thus, such a conduction pattern of heat in the channel walls would provide an explanation for the shape of the saturation curve given in Figure 14. Figure 13 is a plot of recorded centerline temperatures (T_{ℓ}) inside the porous bed and along the outside wall of the test channel (T_w), and Figure 14 shows the saturation variation through the porous bed as measured by the meters. These curves show the temperature of the liquid at the center of the porous bed to be 218 °F in

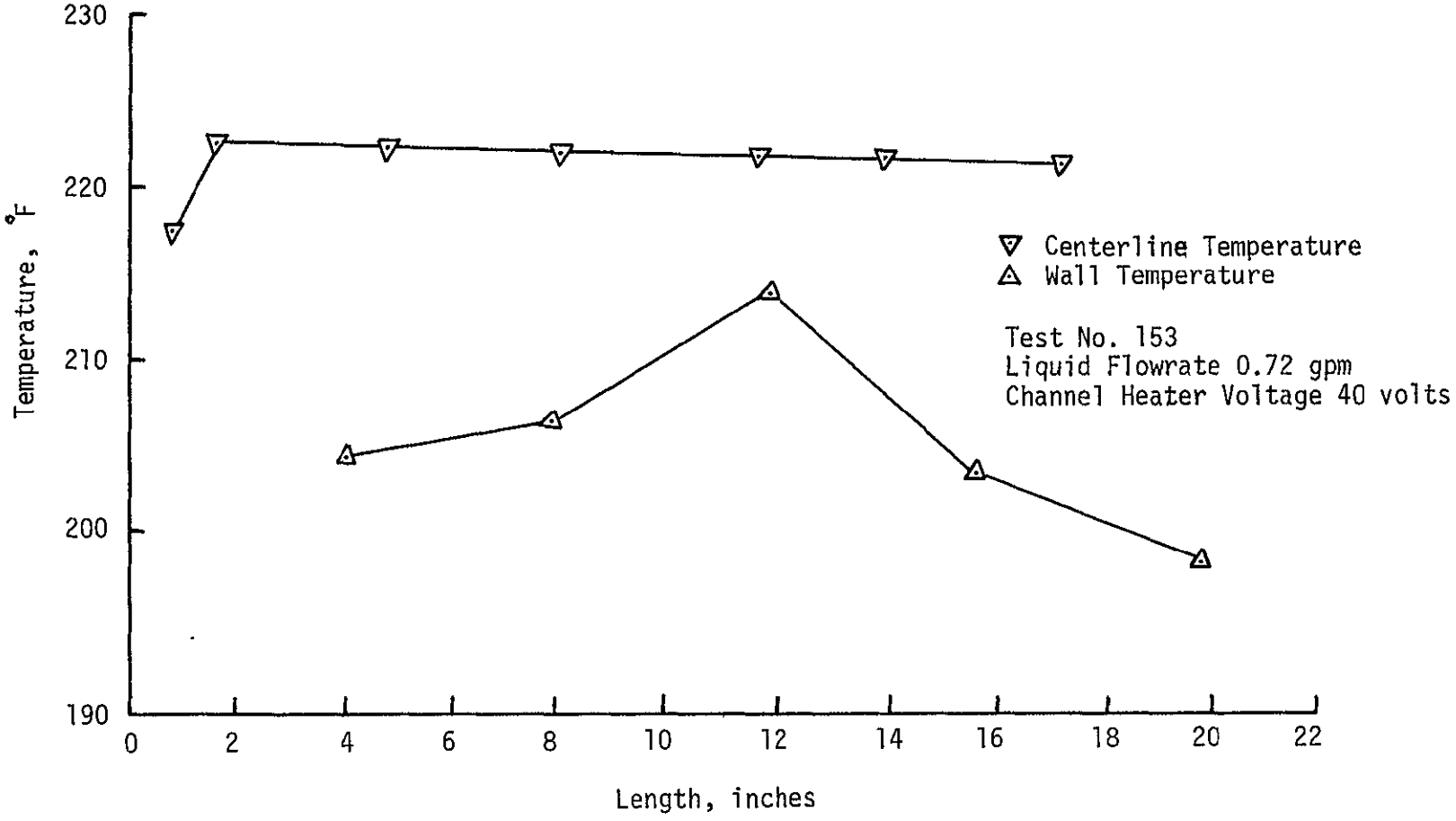

Figure 13. Temperatures at the Centerline of the Porous Bed and Outside the Channel Wall

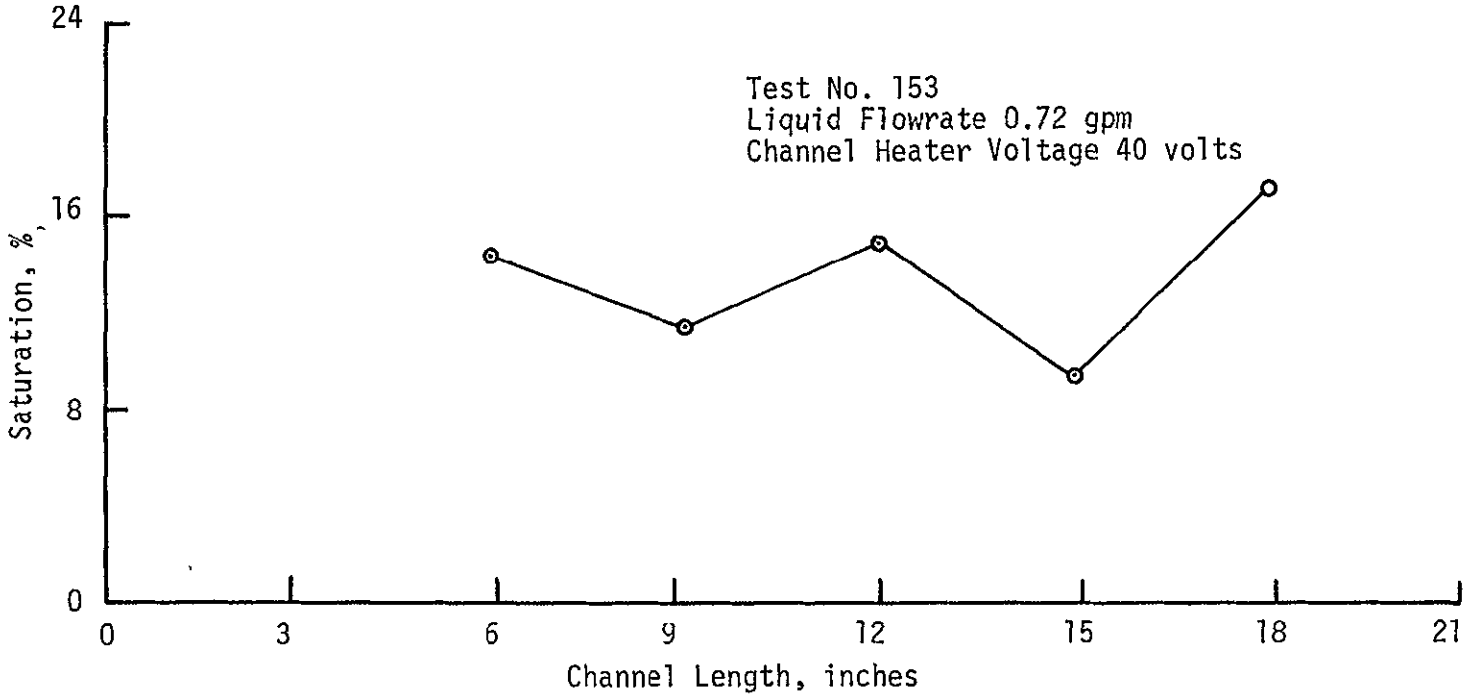

Figure 14. Saturation Versus Channel Length

the region preceeding the heater and 223 °F following the heater and remaining almost constant thereafter. The temperature distribution in the complete channel taken during a typical test is shown in Figure 15. The life of a vapor bubble would be greater along the centerline due to the constant temperature and a decrease in the local pressure as the bubble traveled through the flow field. This would account for the central core region where the vapor flow appeared to be very near that of slug type flow. The constant centerline temperature reinforces the assumption used when deriving the expression for the effective thermal conductivity, that is, the heat transfer in the fluid and porous medium is predominantly radial. When the power was suddenly removed from the heaters a clear liquid front could be observed moving slowly up the channel. Behind the front, the saturation was zero. Ahead of the front, the saturation appeared to be the same as it was immediately before turning off the heaters. The elapsed time for the front to travel the length of the channel was approximately one minute for low flowrates. A qualitative explanation of this can be given in terms of cooling of the aluminum channel. The aluminum walls lose heat to the water first in the lower part of the channel, meanwhile the upper part of the channel walls retain enough heat to maintain vaporization. The cooling of the channel walls progressed upward and took about one minute for vaporization to be completely stopped.

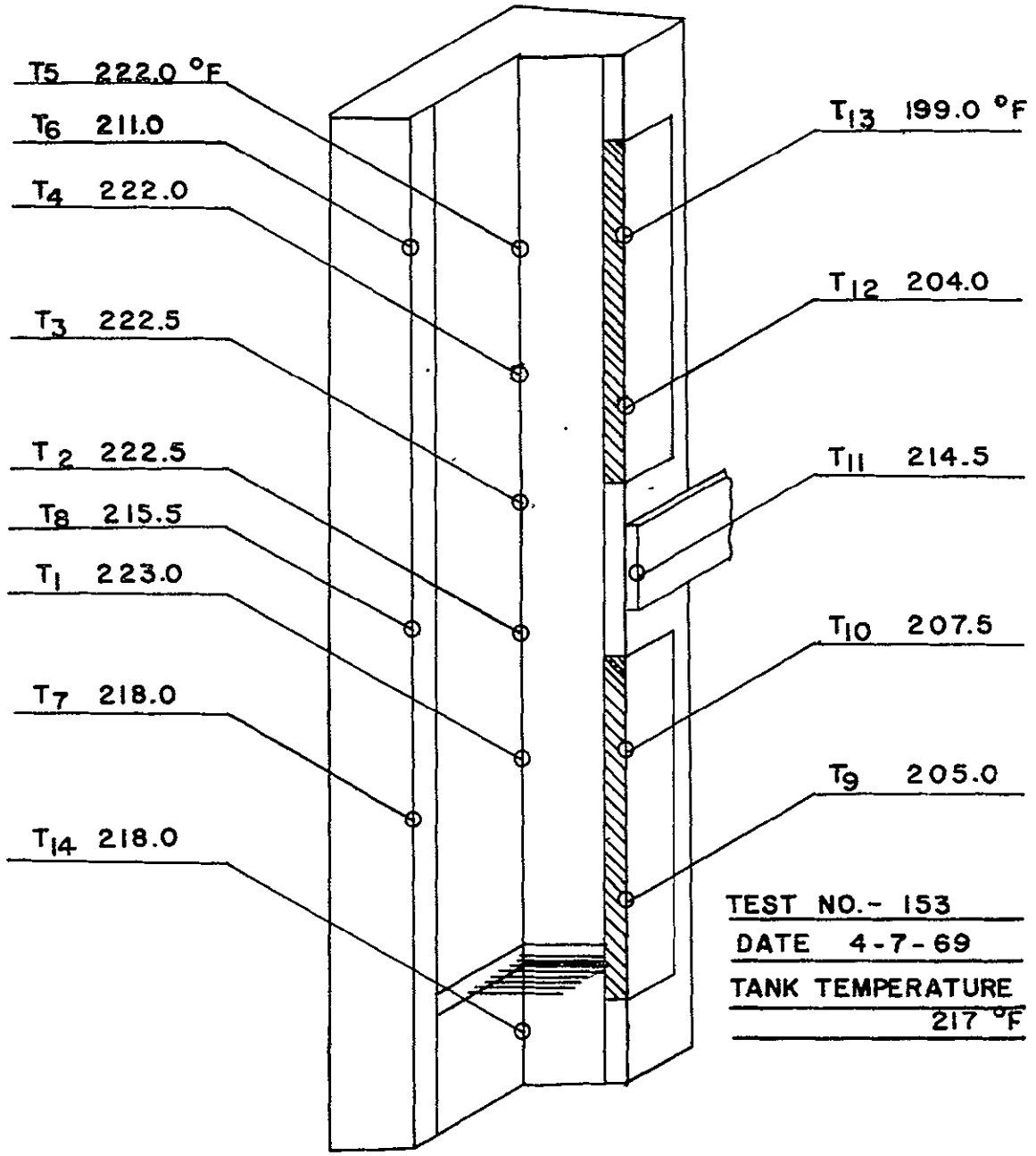

Figure 15. Temperature Distribution for a Typical Test

Another group of tests was run with the Pyrex glass windows replaced by aluminum blanks. Of course, with the aluminum plates attached to the channel, it was not possible to visually observe the flow pattern. The results of a typical test is shown in Figure 16. The significant difference in the two groups of tests is the difference in the saturation curves. The absence of the glass windows eliminated the low values of saturation which occurred in the first group of tests. The aluminum plates were installed in order that the inside wall temperature would approach constant values. This was approximately accomplished as is evident from the curves.

The temperature distribution along the length of the channel was about as expected. The centerline temperature increased sharply across the heater coils and dropped linearly approximately 2 °F to the channel exit. This temperature differential was slightly less than that for the first group of tests (Pyrex glass plates on the channel). The inside wall temperature of the three inch side increased more rapidly than did that of the two inch side and also reached a higher temperature for a given heater condition.

The average saturation increased as the vapor bubbles traveled away from the heater when the glass was replaced by aluminum blanks. The saturation as indicated by the

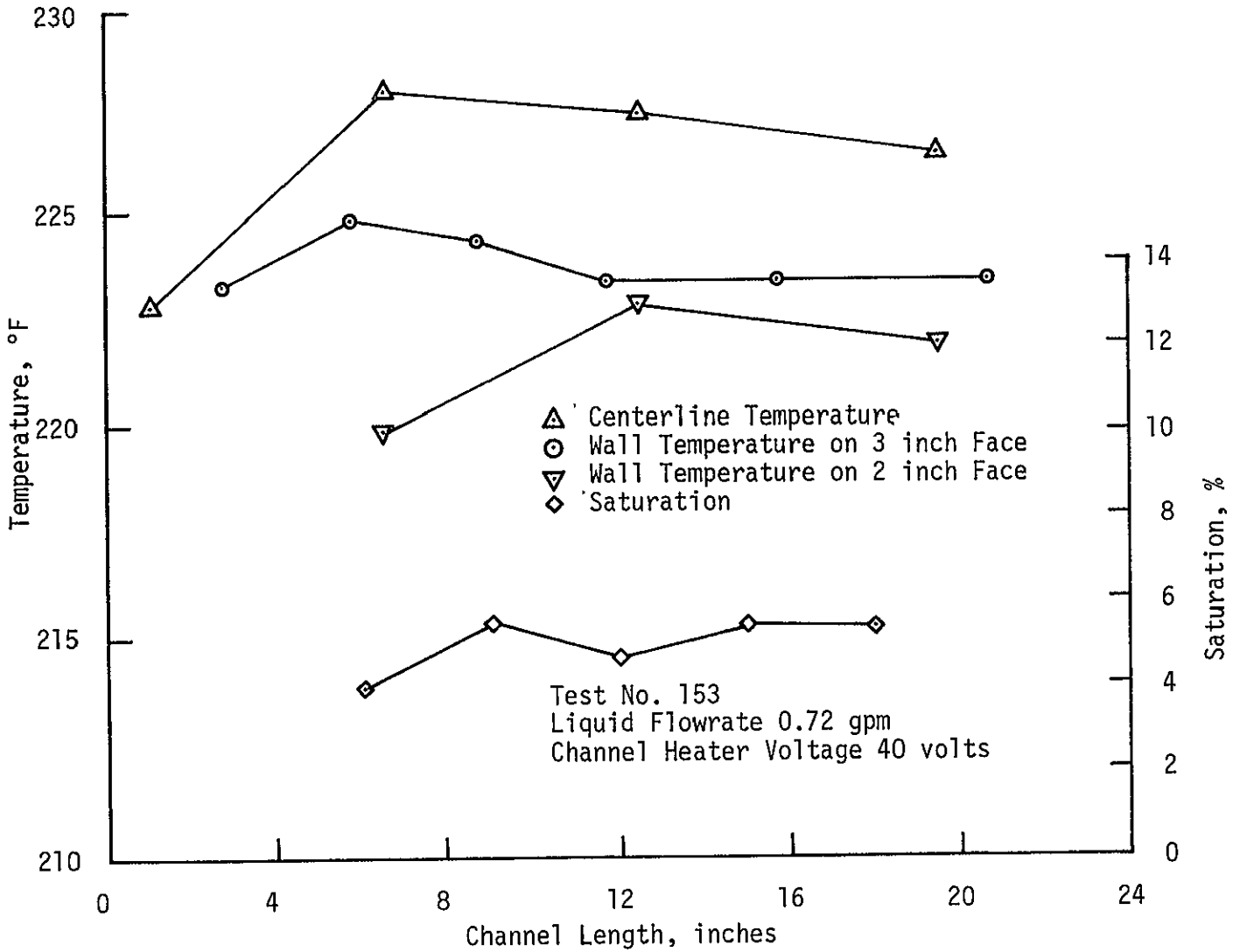

Figure 16. Temperature and Saturation Versus Channel Length for a Typical Test with Aluminum Blanks

meters was about 1.5% greater at meter No. 2 (nine inches from the channel entrance) than it was at meter No. 1 (six inches from the channel entrance). The pressure drop between the two meters was 2.8 psi which should allow the vapor volume to increase slightly, however this is offset by condensation tendencies since the average temperature at this section was somewhat below thermodynamic saturation for the existing pressure. The increase in apparent gas saturation could result from the method of determining saturation by light dispersion. With glass windows on the channel, vapor bubbles could be seen as they formed on the heater coils and were swept away by the moving liquid. The bubbles were large enough to enclose one and sometimes two glass beads (3 mm diameter). With the aluminum walls, the entire system was at a higher temperature; therefore the life of a vapor bubble under similar conditions was extended. Even so, as a vapor bubble left the heater surface and began its travel through the porous bed, its diameter approached the pore size. The larger bubbles had to break up into several small bubbles forming additional interfaces which dispersed more light and the saturation meter reacted as if the saturation had increased.

An expression for predicting the effective thermal conductivity is given in eq. (28). Due to the geometry and composition of the test channel when containing glass windows, one cannot speak of an overall effective thermal

conductivity for the entire porous bed, but must consider that portion of the heterogenous system in which the parameters influencing the energy transfer can be determined within an acceptable degree of accuracy. For this reason a local effective thermal conductivity was determined for three sections of the test channel, the two sections containing the Pyrex glass and the middle section which was aluminum. As was explained in a previous section, the two inch sides of the test channel contained one inch diameter Pyrex glass windows for the saturation meter. The heat transfer through these small windows was neglected and the entire side treated as a continuous plate of aluminum. The thermal conductivity calculated for these sections with the large windows in place was found to vary in a random manner such that no comparison could be made with previously published results. After the glass windows were replaced by aluminum blanks, the effective thermal conductivity was calculated and compared to that presented by Weekman and Myers [25] who studied heat transfer of a foreign gas (air) and water flow through porous beds packed with spherical beads. The calculated conductivity was within ± 15% of their values (Figure 17). Their work was performed at flowrates higher than those in this study; however their data were extrapolated to include the region of interest.

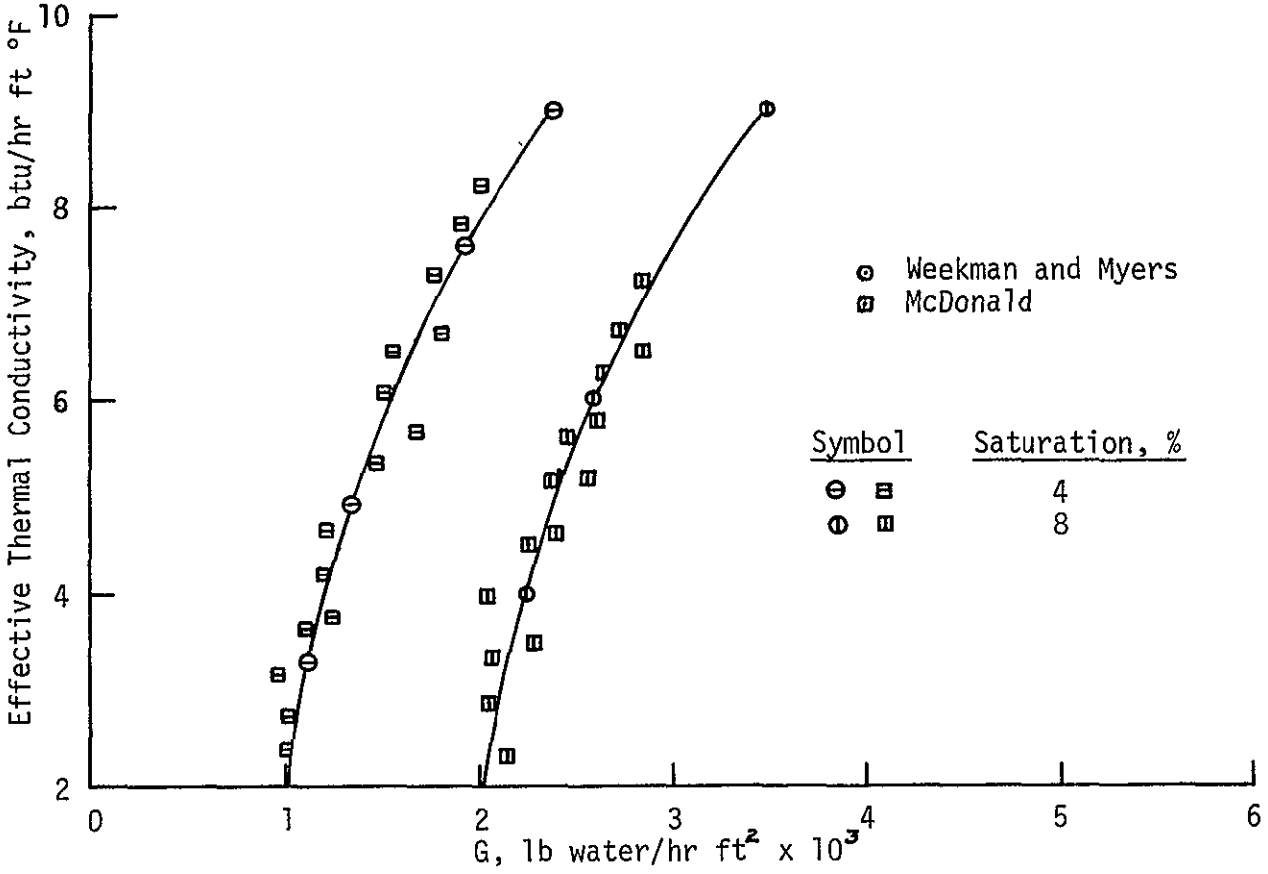

Figure 17. Comparison of Effective Thermal Conductivity with Previously Published Data

It was noted by Henry [7] that when analyzing flow in a porous medium on the basis of a continuum model, there is an effective heat diffusion coefficient which is many times greater than the composite molecular diffusion coefficient. This is shown to be true if the effective thermal conductivity, eq. (28), is subdivided into components representing the amount contributed by each mode of heat transfer. For example at one section of the flow channel, the heat transfer by conduction contributed 18%, and the lateral transport 82%.

No attempt was made to formulate an analytical expression to predict the two-phase pressure gradient for the particular experimental arrangement. One method of approach is to integrate one of Maxwell's relations,

$$\left(\frac{\partial P}{\partial T}\right)_v = \left(\frac{\partial s}{\partial v}\right)_T \tag{31}$$

between the saturated-liquid and saturated-vapor state, the result being the Clapeyron equation:

$$\frac{dP}{P} = \frac{h_{fg}\, dT}{RT^2} \tag{32}$$

However in this study, this equation is not applicable, since Maxwell's relation eq. (31) was derived considering a constant temperature process. A thorough search of the literature was made, and no expression was found predicting

the two-phase pressure gradient for non-isothermal flow through porous media of a liquid and its vapor.

Lockart and Martinelli [13] and Weekman and Myers [24] presented data for the two-phase pressure gradient in horizontal pipes and packed beds, respectively. However their results were in terms of dimensionless ratios, in which the two-phase pressure gradient divided by the single-phase liquid pressure gradient was plotted against the single-phase liquid pressure gradient divided by the single-phase gaseous pressure gradient. Their tests were conducted using a liquid (water) and foreign gas (air) where the above mentioned variables could be measured experimentally. They defined the follwoing dimensionless ratios,

$$\Phi_1^2 = \frac{\left(\frac{\Delta P}{\Delta L}\right)_{TP}}{\left(\frac{\Delta P}{\Delta L}\right)_1} \tag{32}$$

$$\Phi_g^2 = \frac{\left(\frac{\Delta P}{\Delta L}\right)_{TP}}{\left(\frac{\Delta P}{\Delta L}\right)_g} \tag{33}$$

and

$$\chi^2 = \frac{\left(\frac{\Delta P}{\Delta L}\right)_1}{\left(\frac{\Delta P}{\Delta L}\right)_g} \tag{34}$$

From these eqs. (32), (33), and (34), χ^2 is a function of Φ_g^2, and Φ_1^2, that is,

$$\chi^2 = \frac{\Phi_g^2}{\Phi_1^2} \tag{35}$$

Therefore, from the data presented, the two-phase pressure gradient could not be calculated, thus no comparison with this data was possible.

Weekman and Myers applied Lockart and Martinelli's dimensionless pressure gradients, which were derived for flow through pipes, to flow through porous beds of a liquid and foreign gas, and presented experimental evidence that there exists an acceptable comparison of pressure drop correlation for the two different flow mechanisms.

The experimental pressure drop for boiling flow through porous media in the present study was compared with eq. (14). The results were remarkably close as seen from Figure 24. Owens applied eq. (14) to homogeneous two-phase flow of a liquid and its vapor through vertical pipes and ignored the term for pressure drop due to change in elevation. His data are also shown in Figure 18. It is probable that the static pressure gradient is negligible compared with the total pressure gradient at large liquid mass velocities. Of course, with small liquid velocities and the bed approaching zero saturation, a static pressure correction would have to be applied as was the case in this study.

Since the Weekman and Myers porous media data compare favorably with the Lockhart and Martinelli data for flow

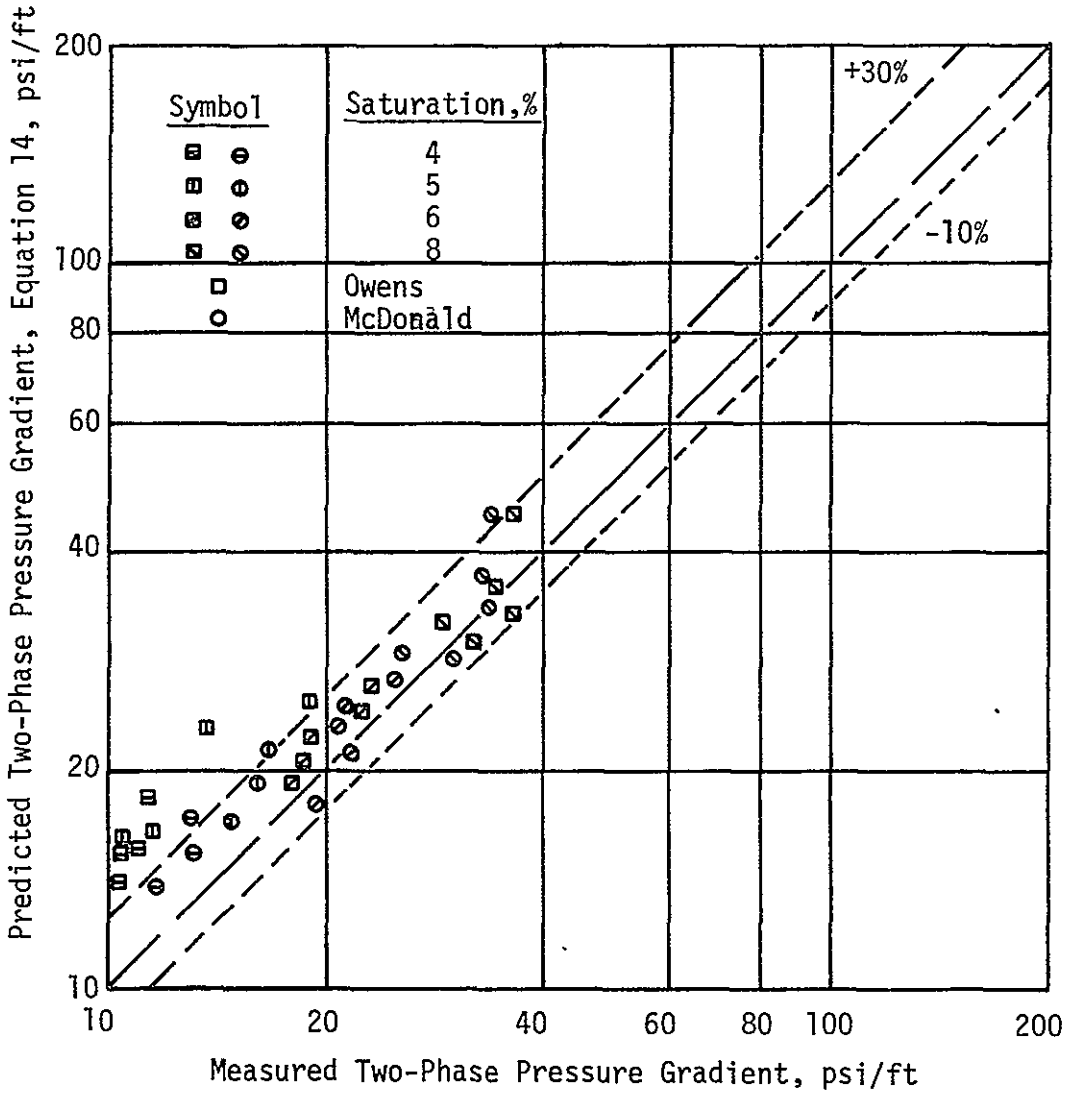

Figure 18. Predicted Two-Phase Pressure Gradient Versus Measured in Vertical Tubes and Porous Media

in horizontal pipes and since data accumulated in the present study compare favorably with Owens data for flow in vertical pipes, it seems reasonable to conclude that a large number of channels in a packed bed function in a manner similar to pipes in two-phase flow.

From the study of data acquired during this study several concluding statements may be made concerning the validity of the results presented herein. For predominantly radial transfer the effective thermal conductivity of a heterogeneous system consisting of a porous material, liquid phase, and vapor phase produced by boiling the liquid may be estimated by the following equation,

$$K_e = (1 - \phi)k_s + [Sk_v + (1 - S)k_l] + \gamma V_0 \rho_l C_{Pl} L\phi \qquad (36)$$

This equation accounts for heat transfer by conduction in the solid, liquid, and vapor, and a convective term for the radial movement of liquid and vapor caused by the tortuous channels in the randomly packed medium. The effective thermal conductivity calculated from data obtained in the experimental tests compared favorably with results of previous investigators.

The saturation of a two-phase mixture can be determined by a measurement of the percentage of light transmitted through the mixture. The saturation at any section in the porous bed was measured by a saturation meter. A separate

experiment was necessary to calibrate each meter (consisting of a light source and photodiode) such that the current output of a photodiode was an indication of saturation. This method could be very useful in determining either the saturation at a particular section or the average saturation in a two-phase flow field in which the thermodynamic properties could not be measured.

APPENDIX A
SUPPORTING EXPERIMENT FOR SELECTING LIQUID AND POROUS MEDIUM

A. PURPOSE

The purpose of this study was to design and test a forerunner to the experimental apparatus that was used in the boiling flow study in order to eliminate unforseen difficulties. At first it was anticipated that a transparent porous bed could be produced such that boiling flow could be studied visually. This required selecting a porous material and liquid which had the same index of refraction and could safely be used in an experiment operating at high temperatures. This was designed to be a pre-breadboard set-up for the earth-orbital flight experiment.

B. SELECTION OF LIQUID AND POROUS MEDIA

At this time it was anticipated that the porous medium would be made by packing Pyrex glass beads into a channel. A fluid survey was conducted in an attempt to find a one component liquid with an index of refraction comparable with Pyrex glass beads and acceptable to be used in a laboratory experiment and space environment.

Some of the more promising liquids found were glycerine, dichloro butanol, fluoro toluene, and triethylene glycol. After detailed library research, glycerine was initially chosen as the best suited liquid; it is a colorless, viscid liquid without odor and miscible with water in all portions. Glycerine has a boiling point of 554 °F at 14.7 psia, a flash point of 734 °F, specific gravity about 1.2, and its viscosity and surface tension decrease with increased temperature. A test was conducted at high temperatures to determine in what way glycerine affects different metals, rubber, teflon, and tygon tubing which were used to fabricate the experimental apparatus. It was found that glycerine had little affect on the metals and teflon but softened rubber. Also, an attempt was made to determine if boiling over long periods of time affects the index of refraction of glycerine.

The glycerine purchased for the experiment was less than 100% pure with unknown thermal properties. An effort was put forth to determine these properties. A tensiometer test was performed to determine the surface tension as a function of temperature. The results were formulated and found to differ approximately 10% from accepted values published in a report by Union Carbide Corporation, [23]. This discrepancy was probably due to the impurities in the tested glycerine.

A sample of glycerine was heated to 400 °F and boiled by an immersion heater. After boiling for several minutes, the glycerine began to discolor. It was found that glycerine polymerizes and decomposes to some extent at this temperature. To reduce the boiling temperature, the possibility of operating the system at a reduced pressure was investigated. This would eliminate the discoloring problems as well as reduce the power necessary to produce boiling. Although glycerine was initially chosen as the working fluid, the study of triethylene glycol was continued in hopes of finding a liquid with more desirable properties. It has a refractive index of 1.456, is less viscous and has a lower vapor pressure than glycerine. Tests were also conducted to determine its corrosive properties and only the rubber materials were affected. Triethylene glycol was selected for the liquid to be used in the pre-breadboard experiment.

Although a bed of Pyrex beads was tentatively selected as the porous medium, the optical quality of the beads received from local distributors was less than desirable. The matching of the refractive index of triethylene glycol and Pyrex was barely acceptable although the beads had internal distortions. It was thought that these distortions were frozen strains formed in the process of manufacturing. Several unsuccesful attempts were made to relieve these strains by annealing.

In order to improve the index of refraction match of the liquid and porous medium, a 96% silica, high temperature No. 7900 ground glass from Corning Glass works was investigated. The indices of refraction of the ground glass and triethylene glycol were 1.458 and 1.4578, respectively. A sample of crushed glass was screened to obtain a uniform particle size; particles passing through No. 12 mesh and retained on No. 20 mesh (sizes from 1.410 mm to 0.833 mm) were selected. One undesirable characteristic of the fused silica was that it exhibited a reddish tint when heated to temperatures above 500 °F, which was below the boiling point (529 °F) of triethylene glycol. Further experimentation with the ground glass revealed that a heat treatment process (700 °F for two hours) would turn the glass first brown and then back to neutral. The index of refraction of the ground glass was unaffected by the heating process. The ground glass proved to be unacceptable, and Pyrex glass beads (3 mm diameter) were selected for the porous medium.

C. PROPERTIES OF TRIETHYLENE GLYCOL

In order to investigate vapor bubbles and heat which is transferred along various solid and liquid paths through a porous medium, it is necessary to have complete knowledge of the heat transfer and thermodynamic characteristics of

the fluid moving through the medium. It would be very helpful if this type information could be obtained from the literature; however such information is not presently available for triethylene glycol. Consequently laboratory tests had to be conducted to determine thermodynamic properties and heat characteristics of triethylene glycol. Limited data on vapor pressure, viscosity and surface tension were obtained utilizing a constant temperature bath shown in Figure 19. The vapor pressure was determined by use of an isoteniscope. The numerical values of vapor pressure were indicated by a Stokes McLeod gage capable of measuring pressures down to one micron of mercury.

The viscosity of triethylene glycol at different temperature levels was determined by pumping liquid from the constant temperature bath through a Hoppler Precision Viscosimeter. The viscosity was calculated as a function of the time required for a calibrated glass ball to drop a constant distance through a tube filled with triethylene glycol.

Surface tension values were obtained by use of a Cenco tensiometer placed in the constant temperature bath.

D. EXPERIMENTAL APPARATUS

The parameters to be experimentally determined in this experiment were: pressures at channel entrance and exit;

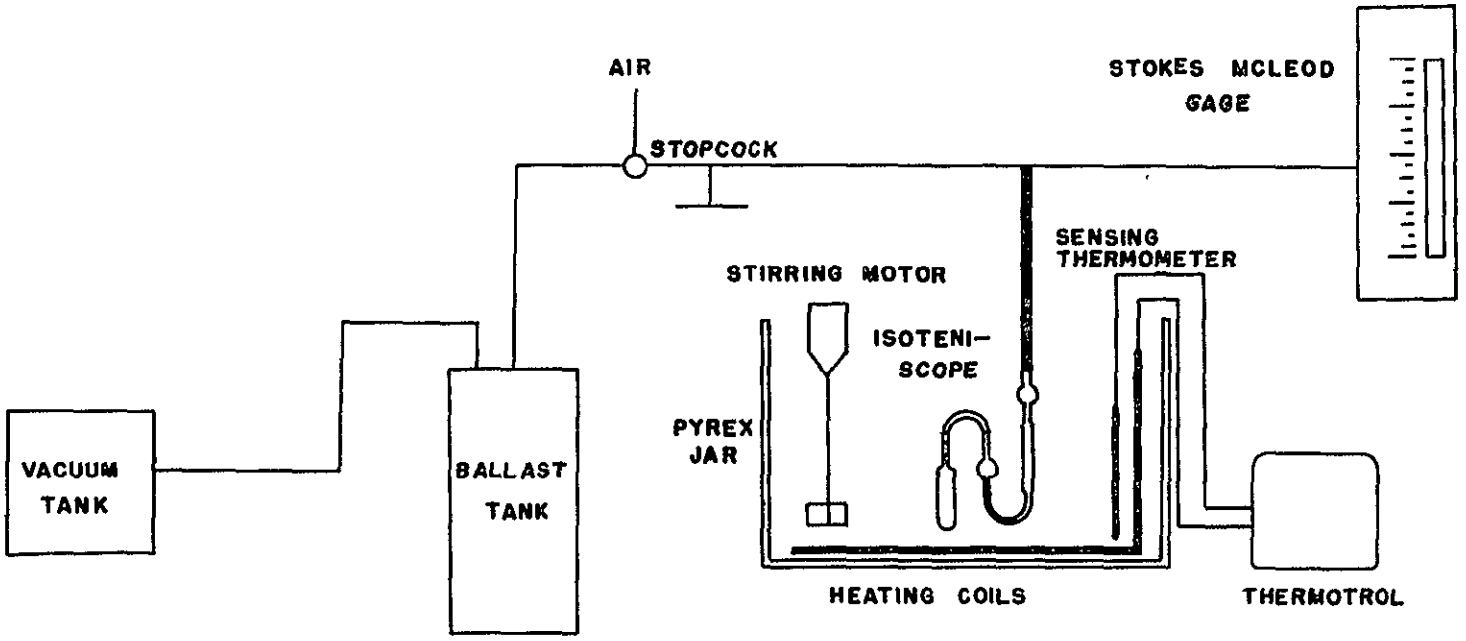

Figure 19. Schematic Diagram of Experimental Setup for Determining Vapor Pressure of Liquids

temperatures in the reservoir and 4 locations within the porous bed; volumetric and mass flowrates; and bubble shapes and characteristics utilizing photography.

The experimental apparatus consisted of a reservoir, pump and motor, heaters with controls, flow meter, pressure gages, thermocouples and temperature recorder, and a channel containing porous beads. A schematic diagram is shown in Figure 20 and pictured in Figure 21.

Triethylene glycol was pumped from the reservoir into a 1 1/8 inch I.D. pipe tee and passed either through a bypass valve back into the reservoir or into the system. Entering the system, the liquid passed through a temperature sensing element, into a pipe containing heaters, flow meter and then into the channel containing the porous medium. Upon entering the porous bed the liquid was boiled and the two-phase mixture traveled through the bed and back into the reservoir.

The channel (Figures 22 and 23) was constructed of 1/4 inch aluminum plate. The inside cross sectional dimensions were 2 inches by 3 inches by 18 inches. Pyrex plates 2 inches by 1/8 inch by 15 inches were placed in slots on each vertical side of the channel. Internal pressure within the channel pressed the glass plates against a neoprene gasket which was held in place by RTV-106 silicone rubber sealant. The end plates of the channel extended into the porous bed 2 1/2 inches at the entrance and 1 1/2

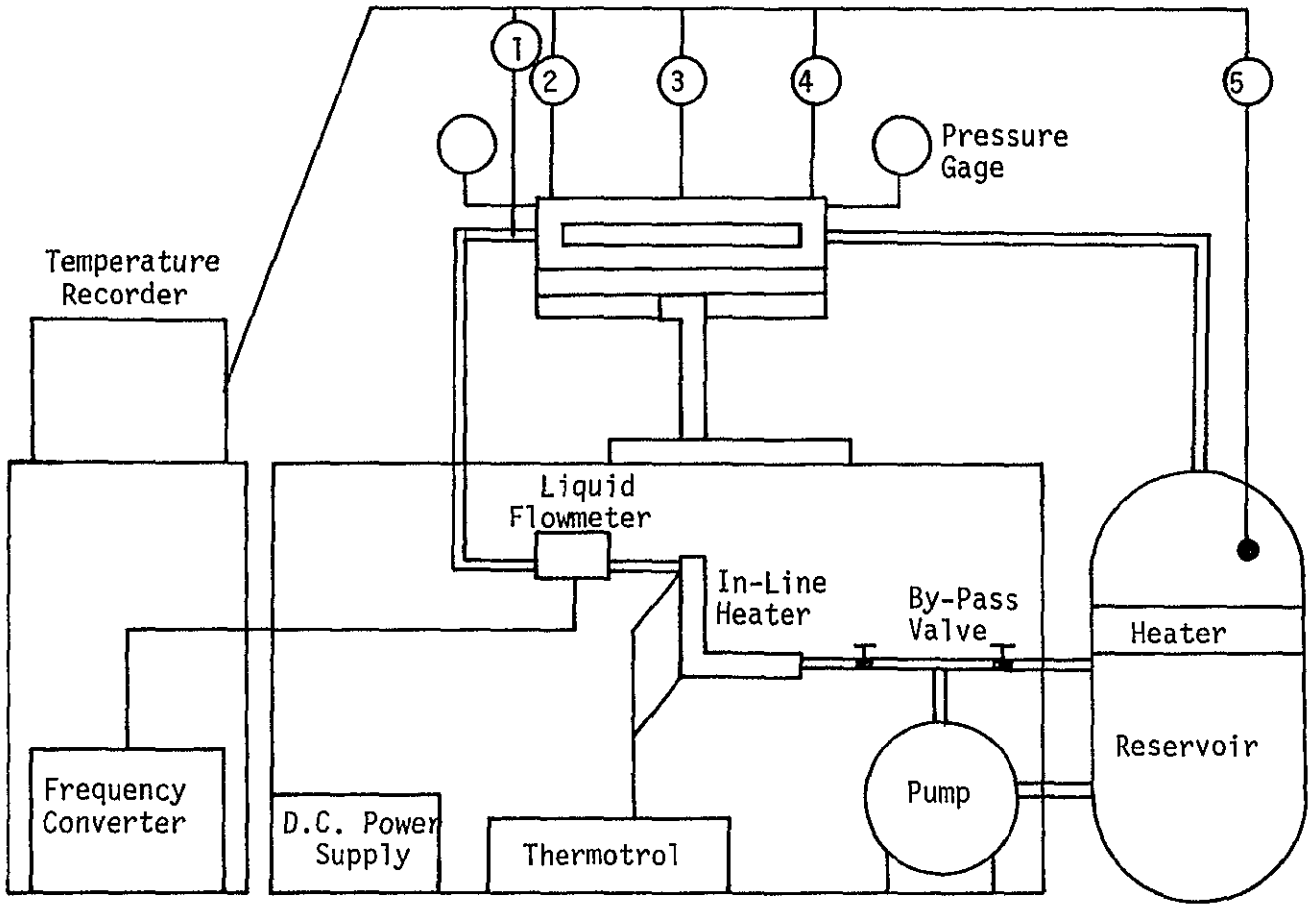

Figure 20. Experimental Apparatus for Studying Boiling Flow of Triethylene Glycol

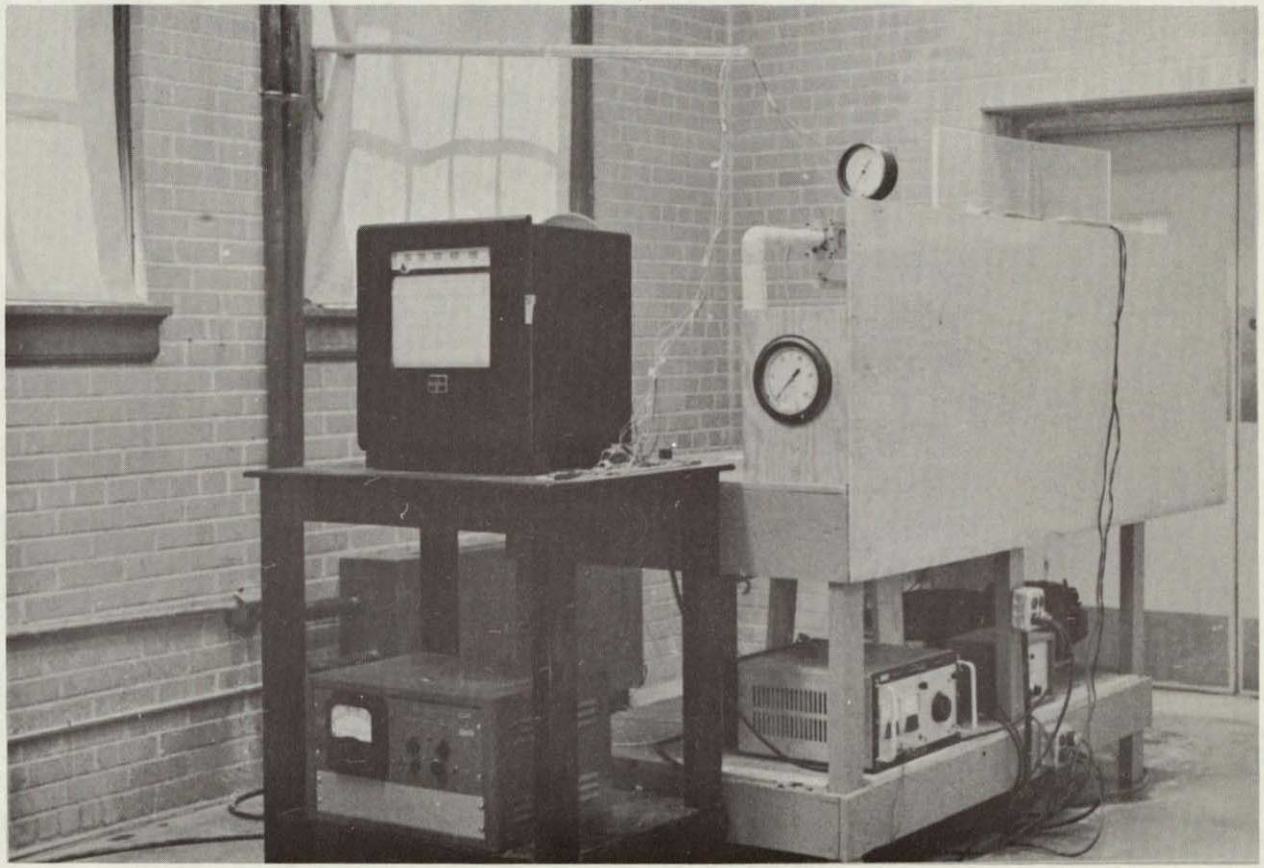

Figure 21. Experimental Setup

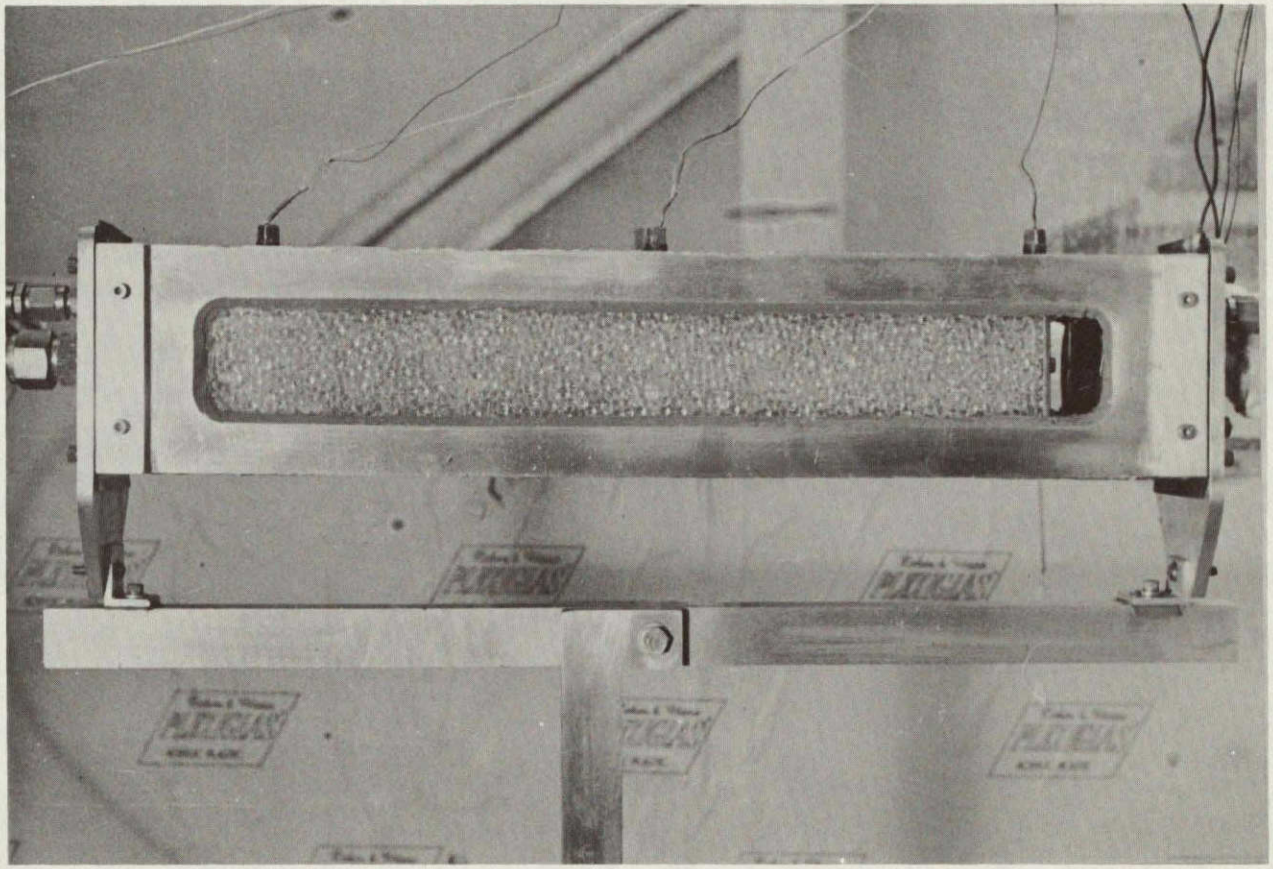

Figure 22. Channel

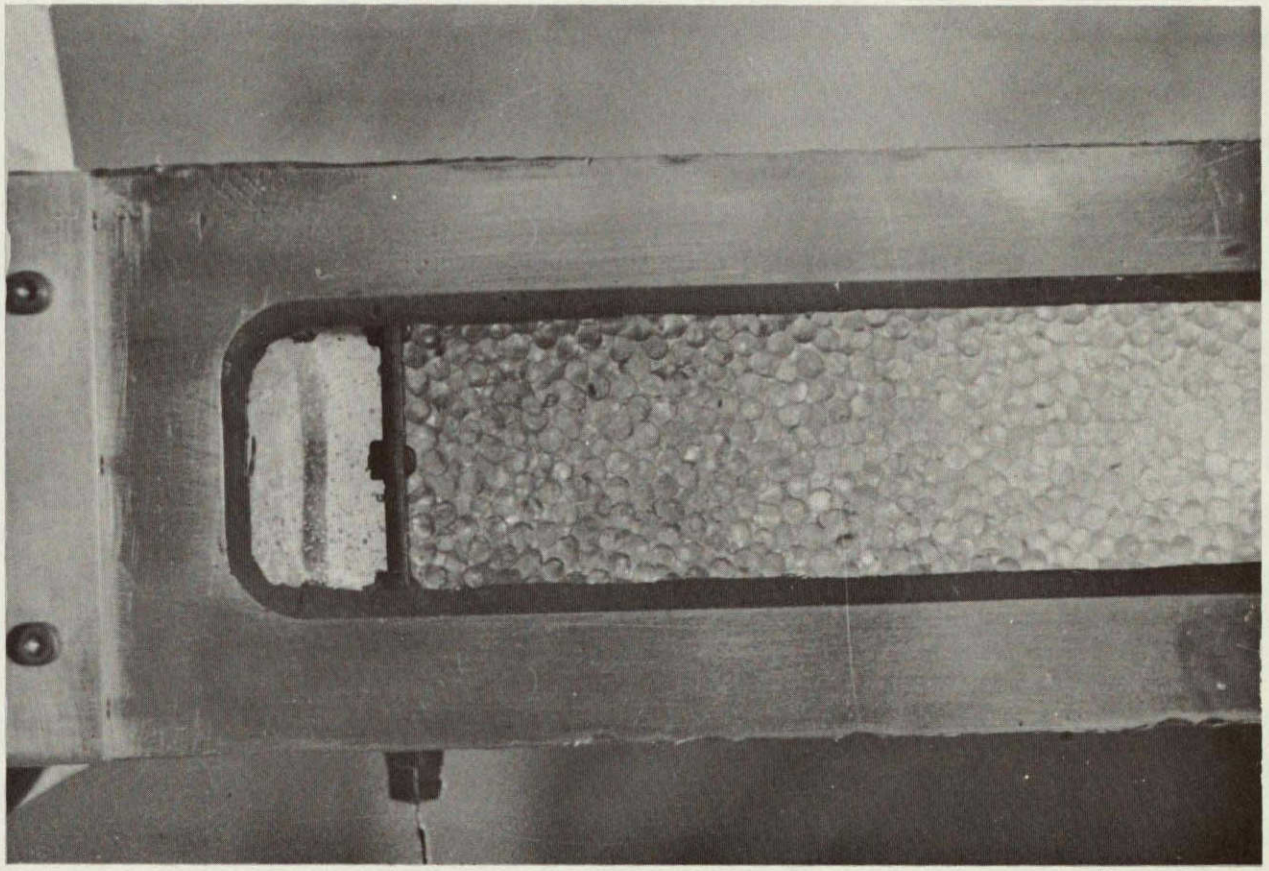

Figure 23. Channel Entrance

inch at the exit, making the porous bed 14 inches in length. A screen on each end plate retained the porous medium. The tubing throughout the system, except for the internal heaters and sensing element, was 1/2 inch O.D. stainless steel connected with Swagelok fittings.

Two separate systems of pre-heaters were installed to initially heat the bulk liquid and maintain the system at its working temperature (approximately 500 °F). One heater system consisted of two 800-watt heaters mounted on a 9-gallon capacity stainless steel reservoir tank. The other employed two 1000-watt immersion heaters silver brazed into a copper tube placed in the flow line. Both systems were controlled by a Thermotrol Temperature Controller Model 1053 with a resistance thermometer sensing element Model No. 1080.

A Deming internal rotary gear constant displacement pump Model No. 1535 driven by a one horsepower Leland electric motor with variable speed capabilities from 800 to 2400 rpm pumped the liquid around the flow circuit. Flowrates were measured by a Potter flowmeter described in a previous section.

The heaters used to produce boiling were coiled 20 ohm resistance wire. They were mounted on the entrance end plate and controlled with a Magitran silicon solid state power supply Model SL 36-12 capable of providing a continuously adjustable output over a voltage range of 0-36 vdc with a maximum current rating of 12 amperes.

Temperatures were measured with copper-constantan thermocouples at five positions within the system: (1) channel entrance, (2) channel entrance upstream of heater, (3) channel mid-length, (4) channel exit, and (5) tank reservoir. The thermocouples were silver soldered into brass plugs which screwed into the top of the channel and sealed with a high temperature (500 °F) epoxy. Because of the high temperature in the system and the corrosive properties of triethylene glycol a problem of maintaining a pressure seal for the thermocouple leads through the channel wall was encountered. The high temperature epoxy used to seal the thermocouple leads would sustain a limited degree of hotness and exposure to triethylene glycol. Temperatures were recorded with a 20-channel Bristol Model 560 wide-strip Dynamaster Pyrometer recording system.

Pressure readings were taken at the channel entrance and exit with a Crosby gage and Test gage, respectively. The Crosby gage had a maximum capacity of 30 psi with 1/4 psi subdivisions, and the Test gage a maximum capacity of 15 psi with 0.05 psi subdivisions.

Because the pressurized system operated at high temperatures, several safety precautions were taken during a test such as: a plywood shield placed along one side of the apparatus separated the operator from the apparatus, and an additional plexiglass shield fastened to the top

of the plywood permitted observation while behind the protection of the shield. The operator wore leather gloves, lab coat, and a welder's helmet with a clear glass view plate to safeguard against burns in the event of failure.

Upon initiation of the flow system, the triethylene glycol completely filled the porous bed and the visibility through the channel windows was excellent. The heaters were turned on and the temperature of the system increased at a rate of approximately 2 °F per minute. When the system reached 160 °F, a number of bubbles were observed flowing through the porous bed. With an increase in temperature these bubbles exhibited a marked increase in size but began disappearing when the temperature reached 250 °F. They were believed to have been air and water vapor originally dissolved in the triethylene glycol. They probably were later trapped in some of the higher portions of the flow circuit or escaped from the vented accumulator tank.

At approximately 250 °F, a slight discoloration of the triethylene glycol was observed. Additional discoloration was encountered with increasing temperature until at 350 °F the porous bed was opaque. The test was continued until the triethylene glycol acquired a black color at 400 °F. At this point a heater connection inside the channel dislodged and the system was shut down. A chemical analysis to determine why the fluid became opaque indicated that the major contaminant was iron along with minor quantities of aluminum, copper and carbon.

The experience and information accumulated during this design, fabrication, and experimentation proved valuable in further work. The channel design used in the boiling flow experiments was modified to incorporate information gathered in this preliminary experiment. Included in these modifications were thicker viewing windows, rearrangement of porous media retaining screens, and thermocouple placement within the porous bed. Also these led to the decision to use water in the boiling experiments rather than glycerine or triethylene glycol.

APPENDIX B
SUPPORTING EXPERIMENTS UTILIZING NITROGEN AND A CARGILLE LIQUID

The purpose of these experiments was to develop and test a fluid flow system which could be used in the study of two-phase flow of a liquid and foreign gas through porous media in an earth-orbital experiment. This experiment provided background for the boiling experiments and also provided a breadboard setup for the foreign gas earth-orbital experiment.

The major components of the system are shown in Figure 24. General operation of the system consisted in pumping liquid from storage tanks (1) with a positive displacement pump (4), filtering the liquid and passing it through a channel (9) packed with flint glass beads. At the same time, nitrogen gas (6) was injected into the channel such that it flowed parallel with the liquid through the bed of glass beads. From the channel this mixture of gas and liquid flowed back to the storage tank and through a screen separator (3) where gas and liquid were separated and the nitrogen released to the atmosphere through a relief valve (2).

The liquid used in the experiment was a light hydrocarbon oil called Cargille Immersion Liquid chosen because of its nonvolatile characteristics and optical properties.

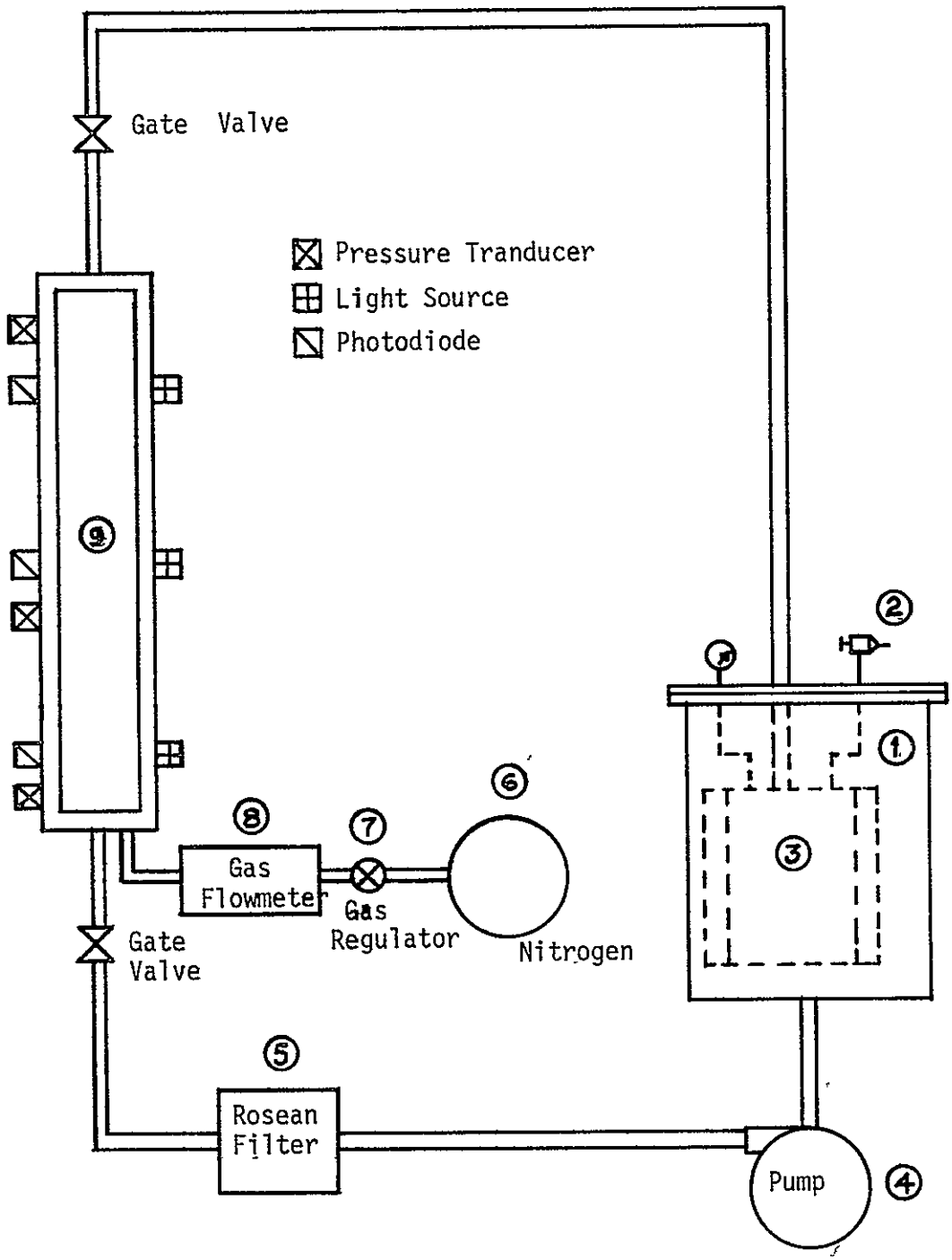

Figure 24. Flow System

Two different mixtures of this hydrocarbon were mixed in proportions of 66:34 to produce a liquid whose index of refraction matched that of the flint glass beads making up the porous matrix. This liquid mixture is a clear fluid similar to water in transparency but oily in consistency. Thus, when the beads were immersed in the liquid they formed a transparent porous bed since the indices of refraction of the fluid and glass were matched. Nitrogen was chosen as the foreign gas because of its inertness and insolubility with respect to Cargille Liquid.

The following is a detailed description of each component of equipment, and an explanation of its operation with respect to the system. The storage tank served a twofold purpose, first, it acts as a reservoir for the Cargille Liquid and second, it provides space for the separation of nitrogen from the liquid after it passes through the channel. This separation process will be discussed later in further detail. The tank was constructed from 304 stainless steel, measuring two feet in diameter, three feet high, and one-fourth inch thick.

The fluid was circulated through the flow circuit by a positive displacement Hydraulic Gerotor pump with a capacity of eight gallons per minute at 1750 rpm. The pump was driven by a direct coupled motor rated at 1/3 hp and 1750 rpm. A rheostat was connected in series with the field circuit of the motor such that motor speed, and

therefore flowrate, could be varied. Out of the pump, the liquid was directed through a cartridge filter (5), and then to the channel entrance.

The channel was constructed of 1/4 inch aluminum plates (inside dimensions 2 inches by 3 1/2 inches) with 3/8 inch glass set into the two sides of largest dimensions. Circular glass disks (one inch in diameter and 1/8 inch thick) were set into 4 equally spaced holes along each of the other two sides of the channel over which were placed photodiodes and opposite to each of them a light source (Figure 25). The channel was packed with 3 mm flint glass beads with an index of refraction which matched that of the liquid, the index being 1.51. Liquid entered the channel through a centrally located opening in the bottom end plate of the channel. Nitrogen was discharged through 8 small ports (Figure 26) into the channel from an injector chamber in the bottom end plate which was connected to a 3/8 inch O.D. gas line. A check valve was placed in this line to prevent liquid from draining back into the gas line.

As nitrogen was injected into the channel, the amount of light incident upon a photodiode was decreased. Hence the amount of gas in the channel at any particular time was proportional to the light intensity reaching the photodiode. Therefore the amount of nitrogen present in the porous bed was calibrated in terms of photodiode output current. The schematic of the photodiode-light source circuit is shown in Figure 25.

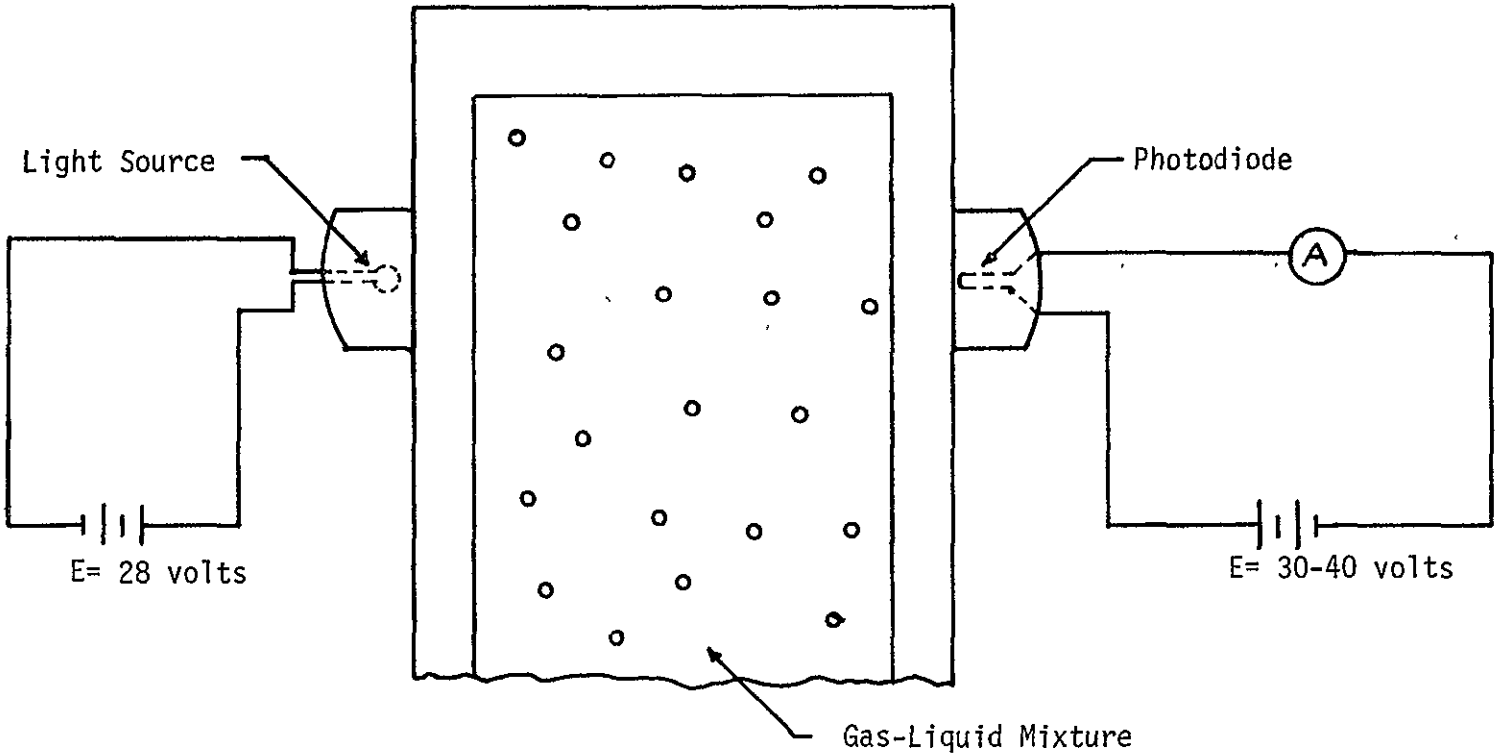

Figure 25. Photodiode-Light Source Circuit

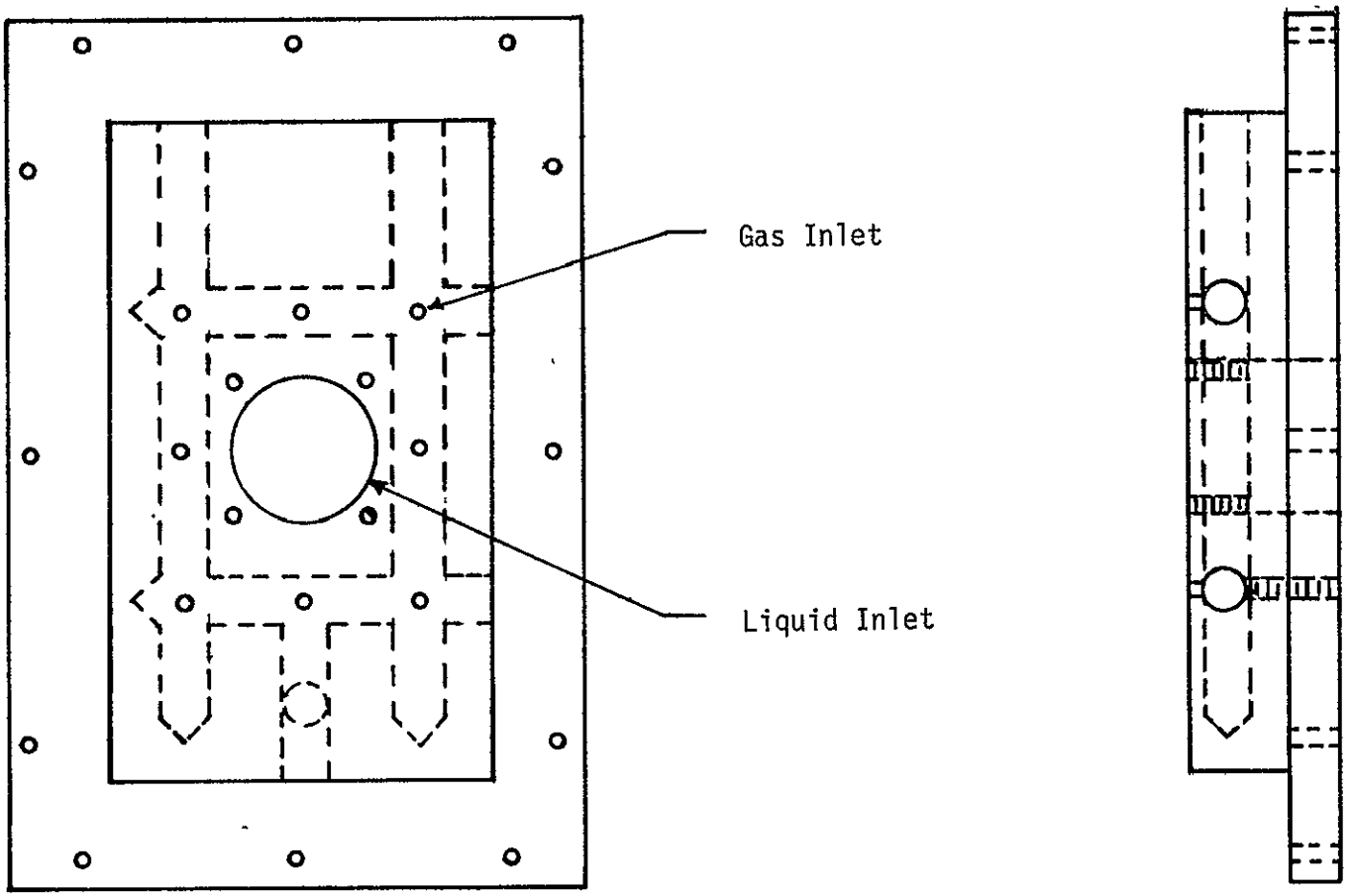

Figure 26. Bottom End Plate and Gas Injector

The nitrogen introduced into the channel was stored in a high pressure cylinder from which it flowed through a converging-diverging nozzle (Figure 27) such that the nitrogen flowrate could be calibrated using the supply pressure and temperature.

The mixture of liquid and nitrogen discharged from the channel was returned to the storage tank which contained a screen separator. The mixture entered the separator beneath the liquid surface. At this point the gas bubbles were filtered from the liquid and escaped through a relief valve while the liquid passed through a screen and remained in the storage tank.

Several pieces of equipment and experimental procedures require clarification as to their effectiveness. These include the screen phase separator, gas flow nozzle, liquid flow metering method, back pressure relief valve, and the use of photodiodes to measure bed saturation.

The phase separator (Figure 28) was constructed from copper sheet and screen consisting of two concentric cylinders made of copper screen, the inner screen being 40 mesh while the outer screen was 60 mesh soldered to copper end plates. The liquid-nitrogen mixture entered the center cylinder where the nitrogen was trapped as a result of capillary attraction and the liquid passed through. The separator performed remarkably well during all tests. No nitrogen bubbles could be observed entraining into the channel,

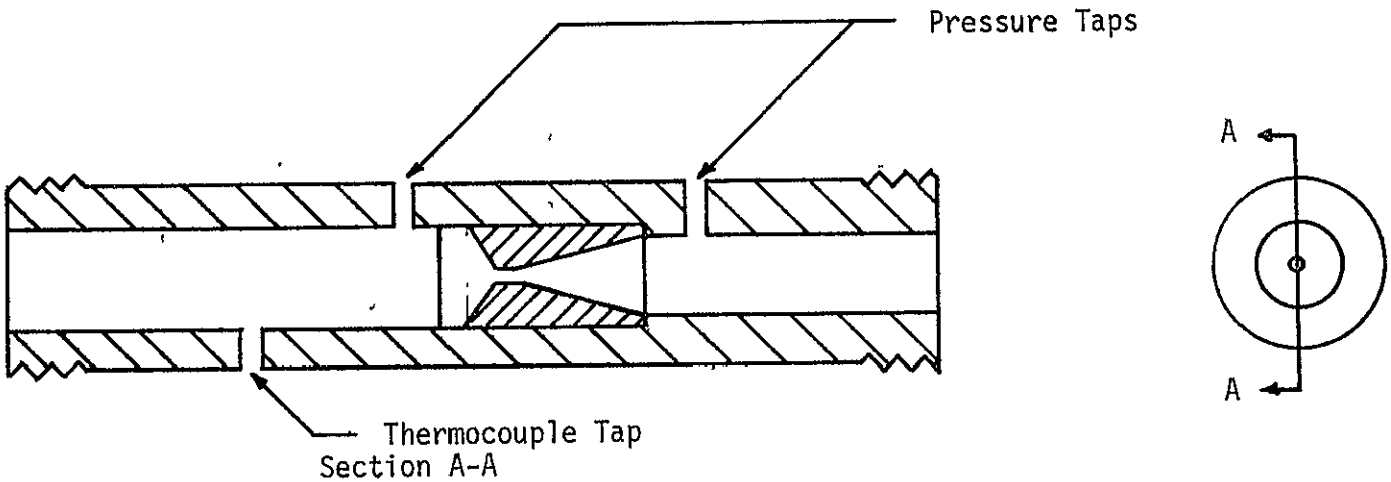

Figure 27. Gas Flow-Metering Nozzle

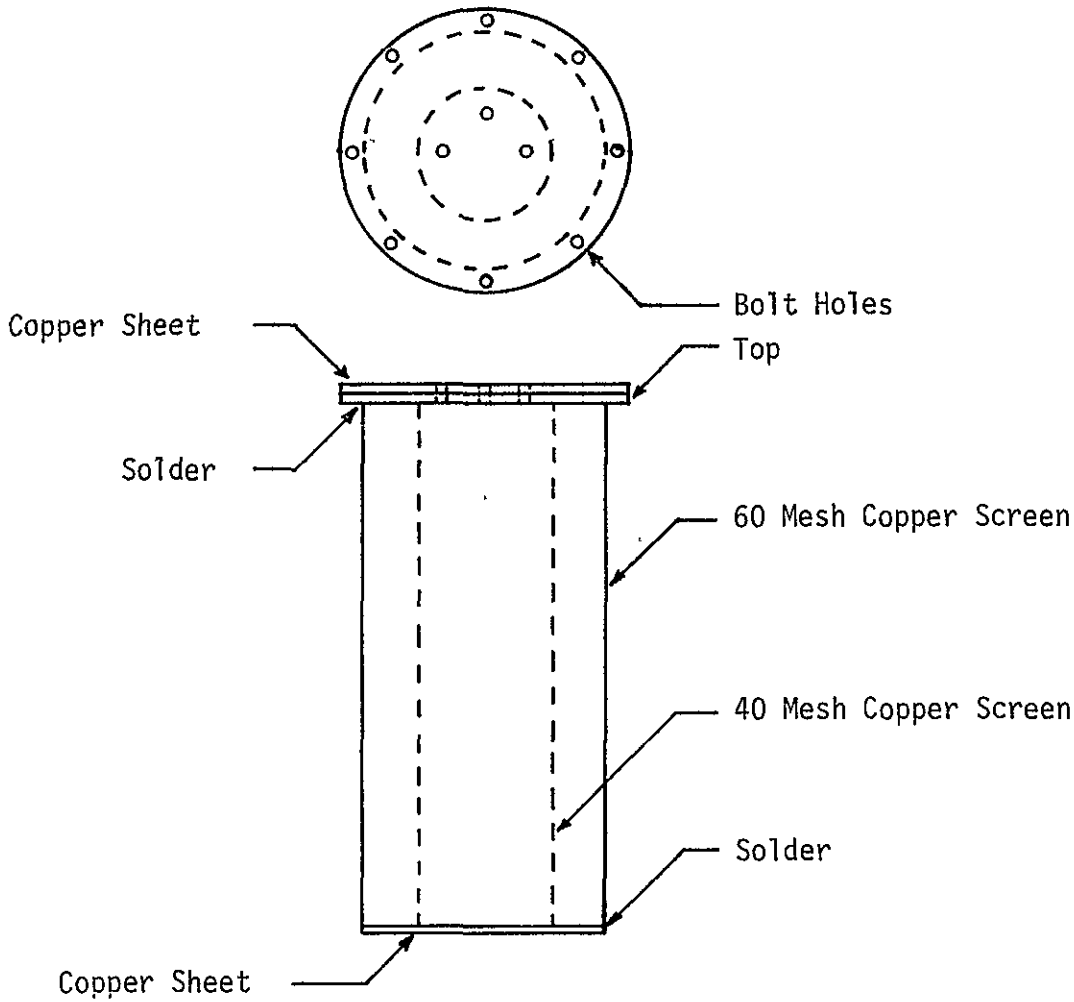

Figure 28. Gas-Liquid Separator

even at high flowrates proving that all of the nitrogen had been separated from the liquid. The large capacity of the storage tank (70.5 gallons) also helped to provide adequate disengaging space and holdup time such that the nitrogen could separate from the liquid by gravity.

The speed of the motor driving the pump was calibrated in terms of liquid flowrate as shown by Figure 29. This was accomplished by using a tachometer to measure motor speed and a bucket and stopwatch to obtain the flowrate. One source of error was that the motor speed did not remain constant because of the inefficiency of the variable speed electrical system and the heating of the rheostat used to control the motor speed. In spite of this error, an excellent calibration curve was obtained as indicated by the linearity of the curve. The affect of back pressure or storage tank pressure on liquid flowrate was determined since it was required that the system be pressurized and operated at about 2 psig. As indicated by Figure 30 storage tank pressure has negligible affect on liquid flowrate.

As was mentioned earlier, the nitrogen flowrate was determined by use of a converging-diverging nozzle (Figure 27). Before the nozzle was calibrated, a plot of maximum back pressure for sonic throat conditions versus supply pressure was made to insure that sonic conditions would be maintained in the nozzle throat during all tests. The

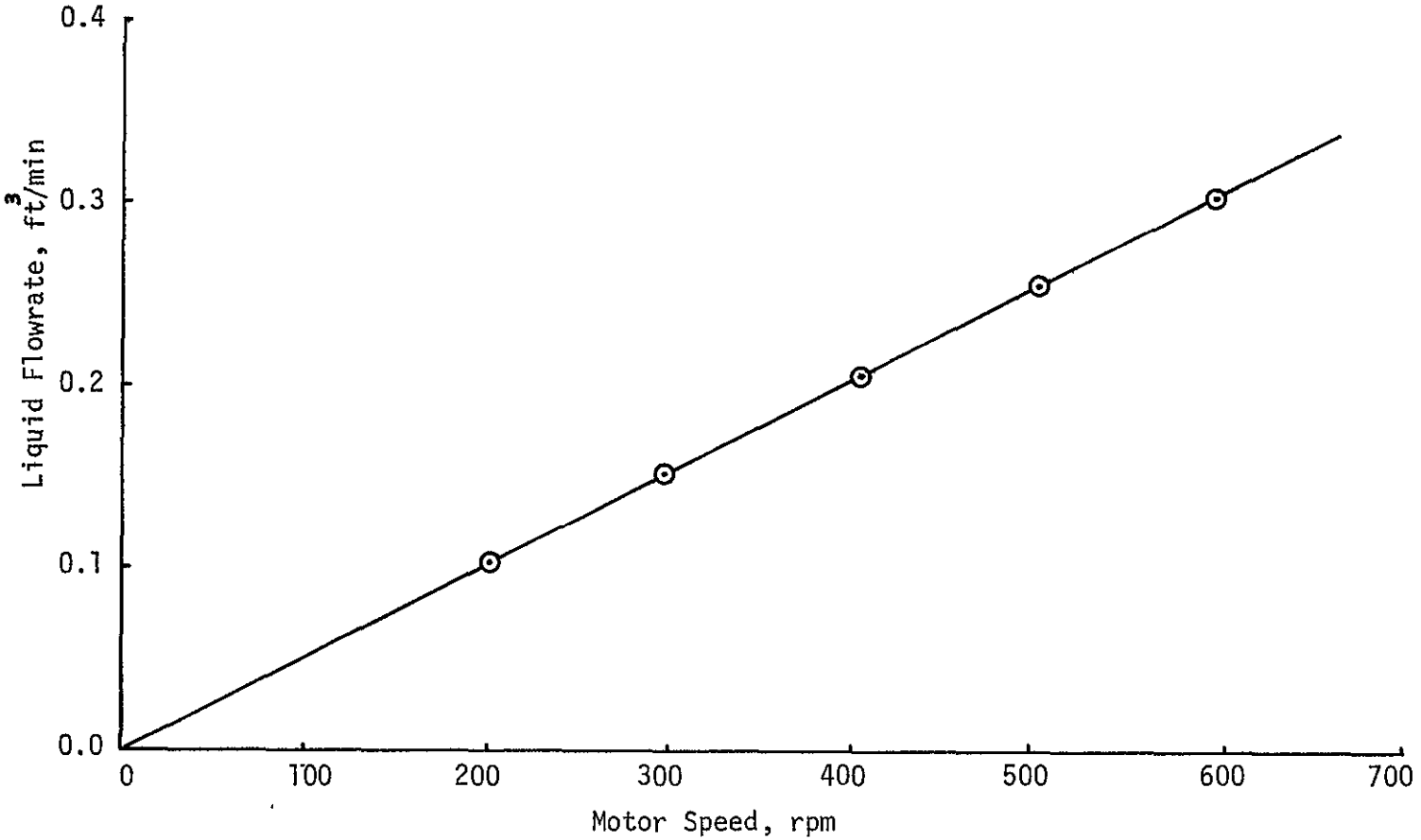

Figure 29. Liquid Flowrate Versus Motor Speed

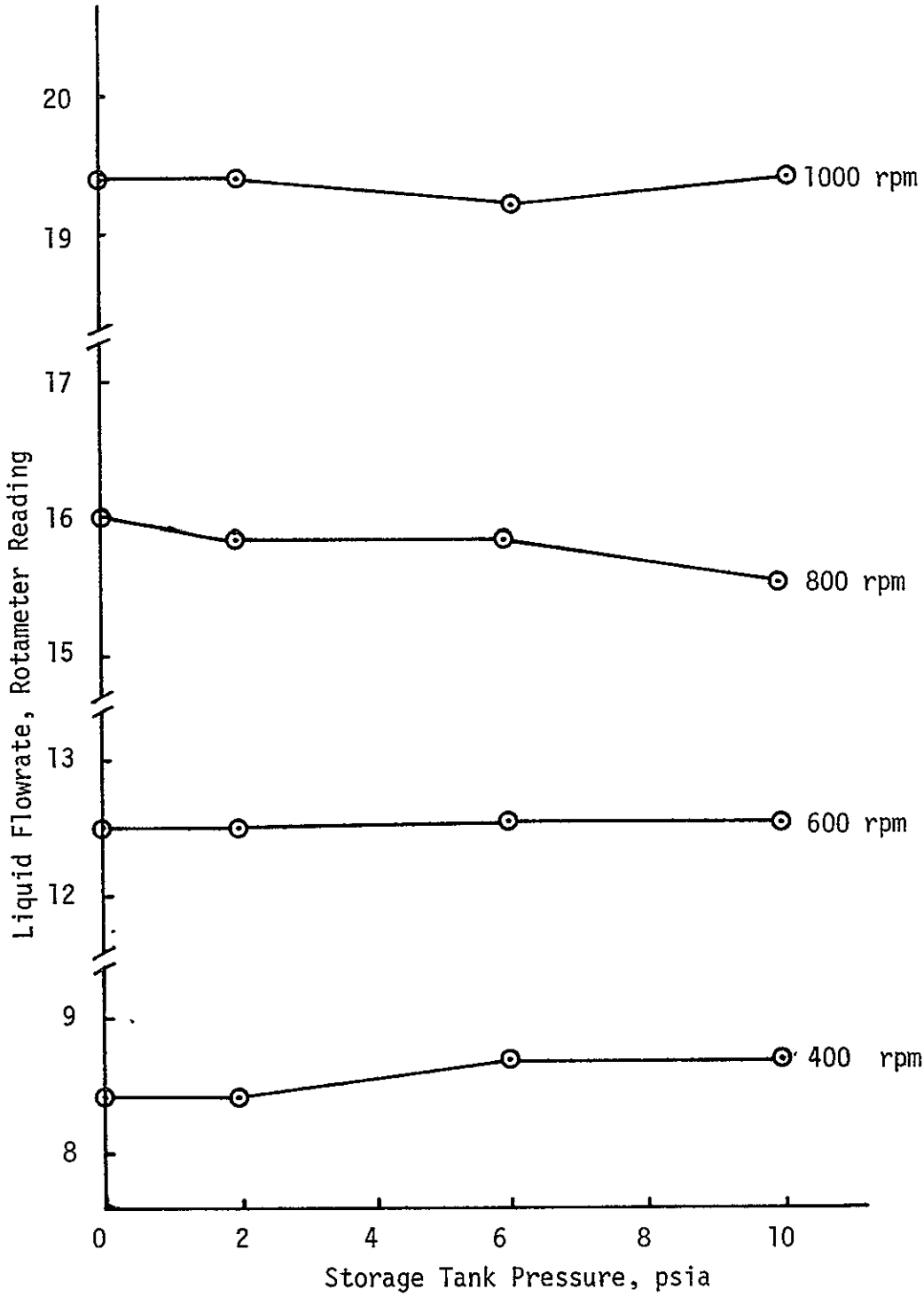

Figure 30. Liquid Flowrate Versus Storage Tank Pressure

results of this test are shown in Figure 31 and an extension of the curve for a supply pressure of 40 psi to 70 psi is shown in Figure 32. This was the principal operating range of the nozzle as used in this system. The actual calibration was made by setting the supply pressure of the nozzle to a predetermined value and allowing the nozzle to exhaust into a large cylindrical plastic bag. By recording the supply pressure, time required to fill the bag to atmospheric pressure, temperature, and measuring the volume of the bag, a plot of nozzle supply pressure versus gas flowrate in cubic feet per minute was obtained (Figure 33). The experimental apparatus for this calibration is shown in Figure 34. Thus the gas flowrate was varied by adjusting the control valve on the inlet side of the nozzle. The calibration curve is linear as indicated by Figure 33. This method of calibration proved to be quite accurate due to the large amount of time required to fill the plastic bag. The only problem was in determining the exact moment the bag was filled to atmospheric pressure. To determine this, an inclined water manometer was used and proved to be adequate as long as the angle of inclination was small, thus making its response very sensitive. Determining the exact volume of the bag was also an important point since it was found that the bag stretched if over inflated.

As stated before, a relief valve was placed on the storage tank to maintain a constant pressure. The one used

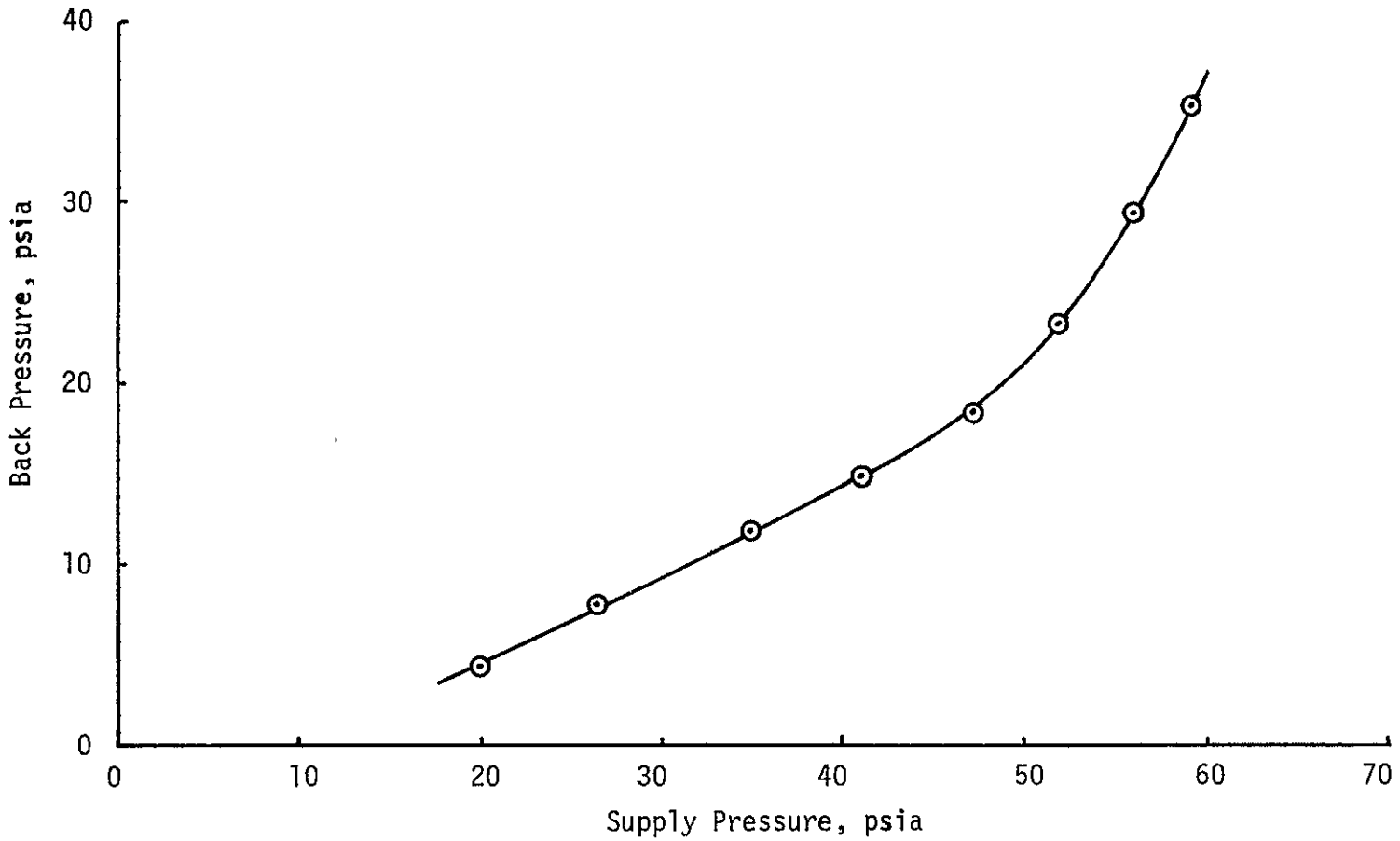

Figure 31. Maximum Back Pressure Versus Supply Pressure for Sonic Conditions

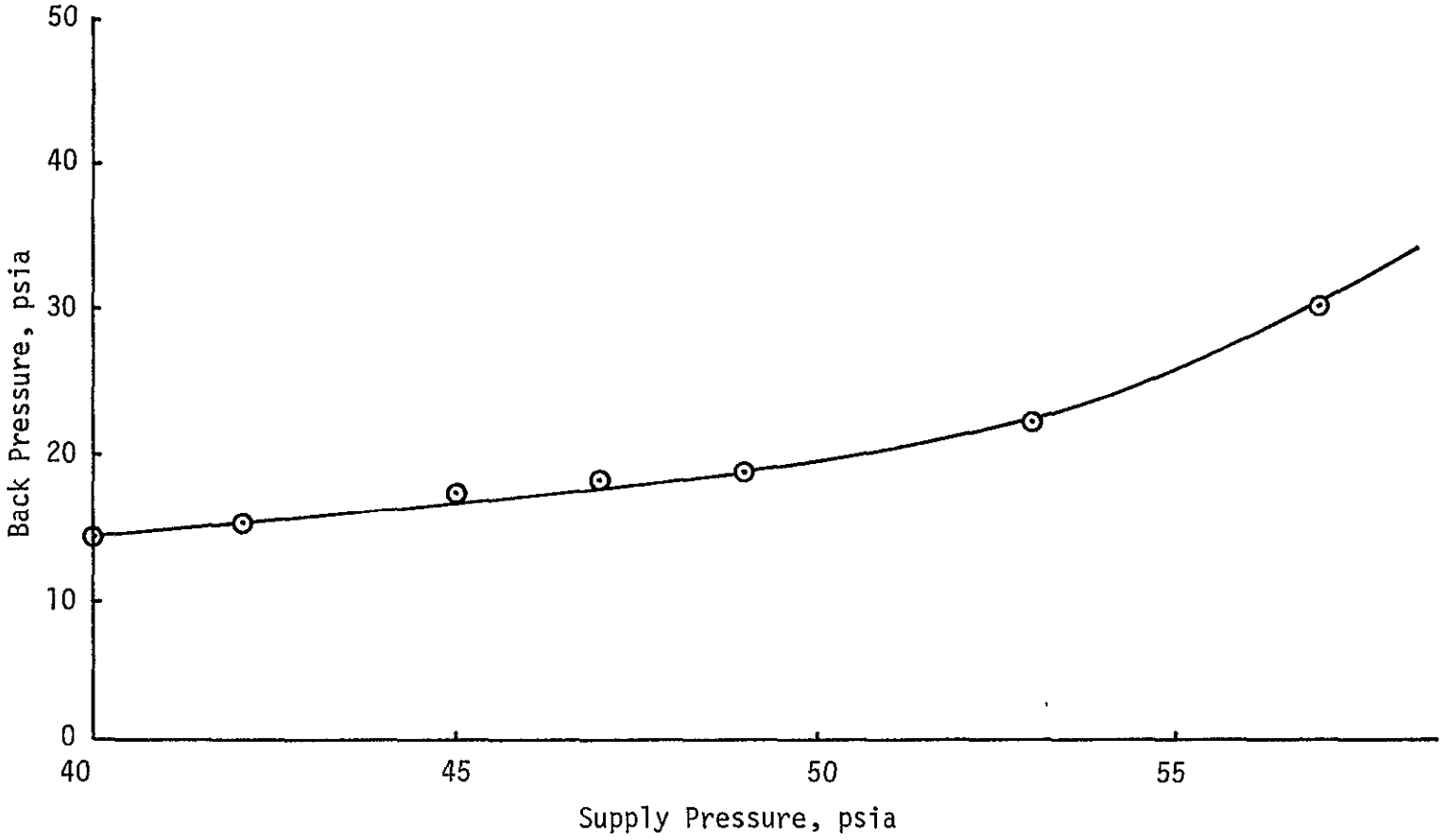

Figure 32. Maximum Back Pressure Versus Supply Pressure for Sonic Conditions

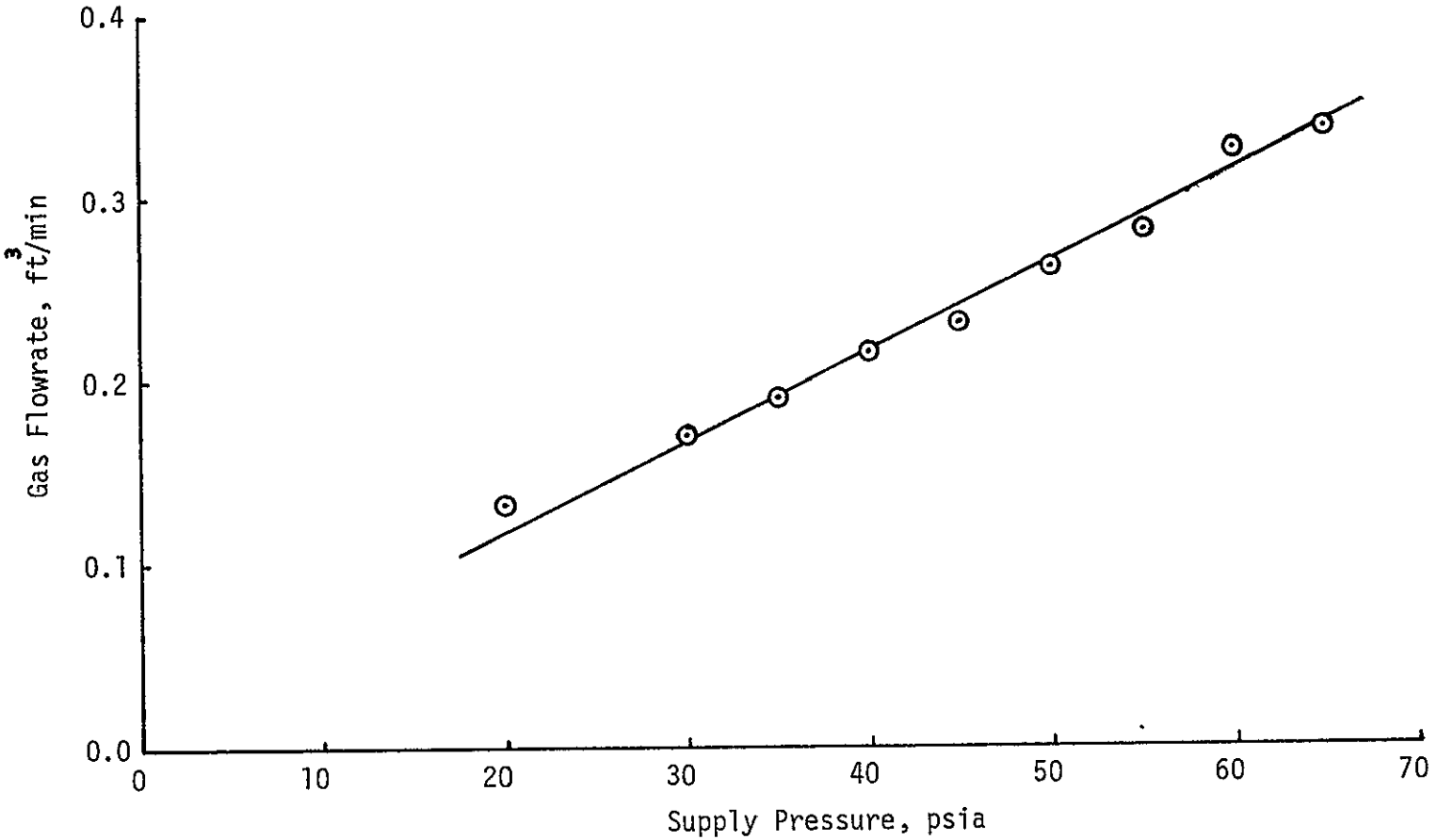

Figure 33. Gas Flowrate Versus Supply Pressure

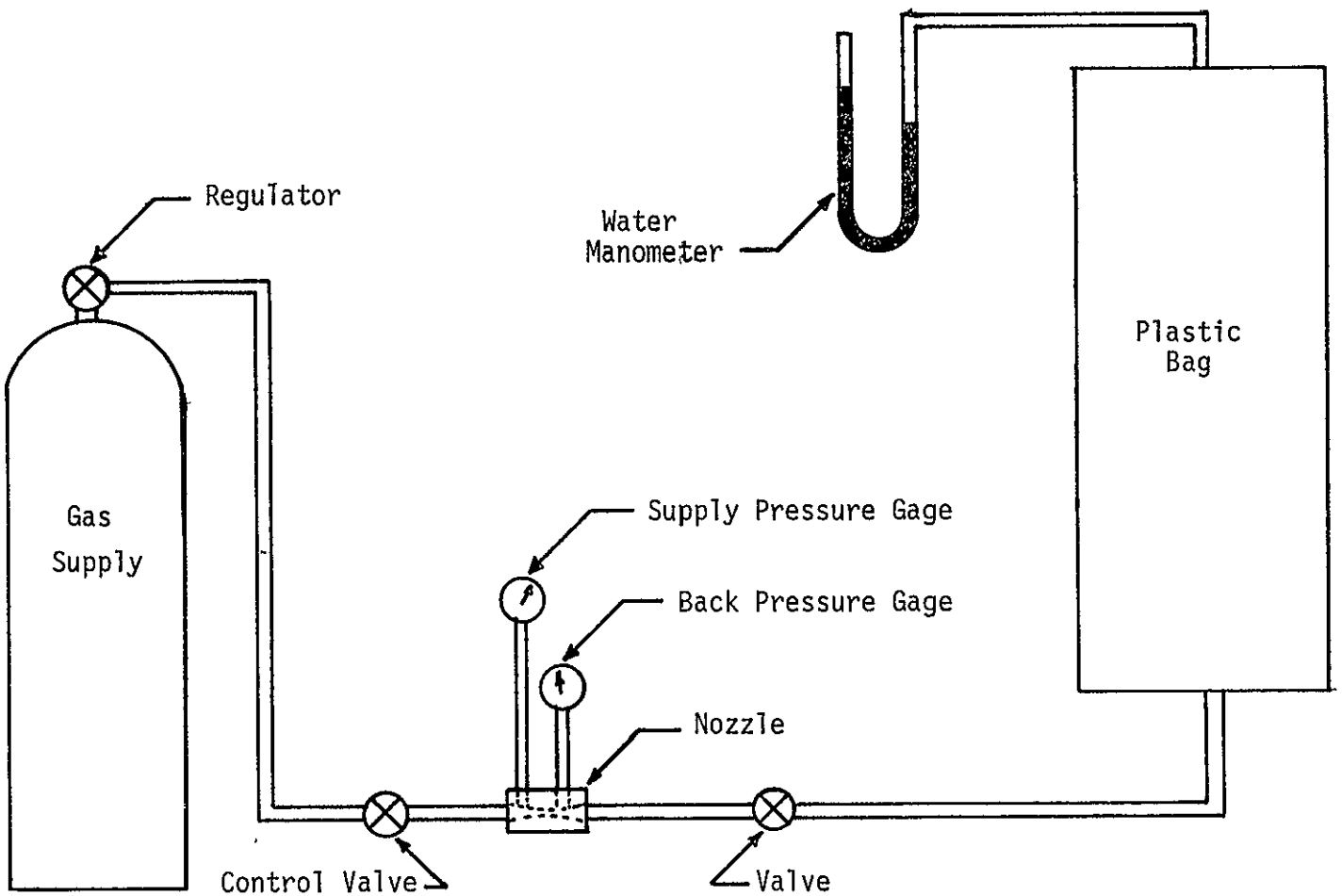

Figure 34. Gas Flowrate Calibration Equipment

in this experiment was an A, W. Cash type BQ diaphram relief valve with pressure range from 0 to 15 psi. The valve did not maintain a constant pressure for all nitrogen flowrates but regulated deviations in the tank pressure within 1 psi. Since the system was not critically dependent on this pressure, the valve worked very well for this purpose.

Saturation meters were used to measure saturation in these experiments. Since Cargille liquid was used as the liquid phase and nitrogen as the gaseous phase, the meters had to be calibrated. The calibration procedure is the same as used in the boiling experiment. To calibrate the photodiode current against the amount of liquid displaced by the nitrogen, the channel containing the porous bed was placed on a Toledo balance scale and balanced such that the scale indicator read the full scale reading of 2.0 lb. Since the channel had the inlet and exit hoses connected, the stiffness of these had to be considered. The correction factor for the hose stiffness was found by placing a known weight on the balance and taking a reading from the scale indicator. The difference in indicator reading and actual weight was then used as the correction factor. The plot of correction factor versus the scale reading is shown in Figure 35. It was observed that the correction factor did not vary in the same manner with increasing weight as decreasing weight, as shown by the hysteresis effect of

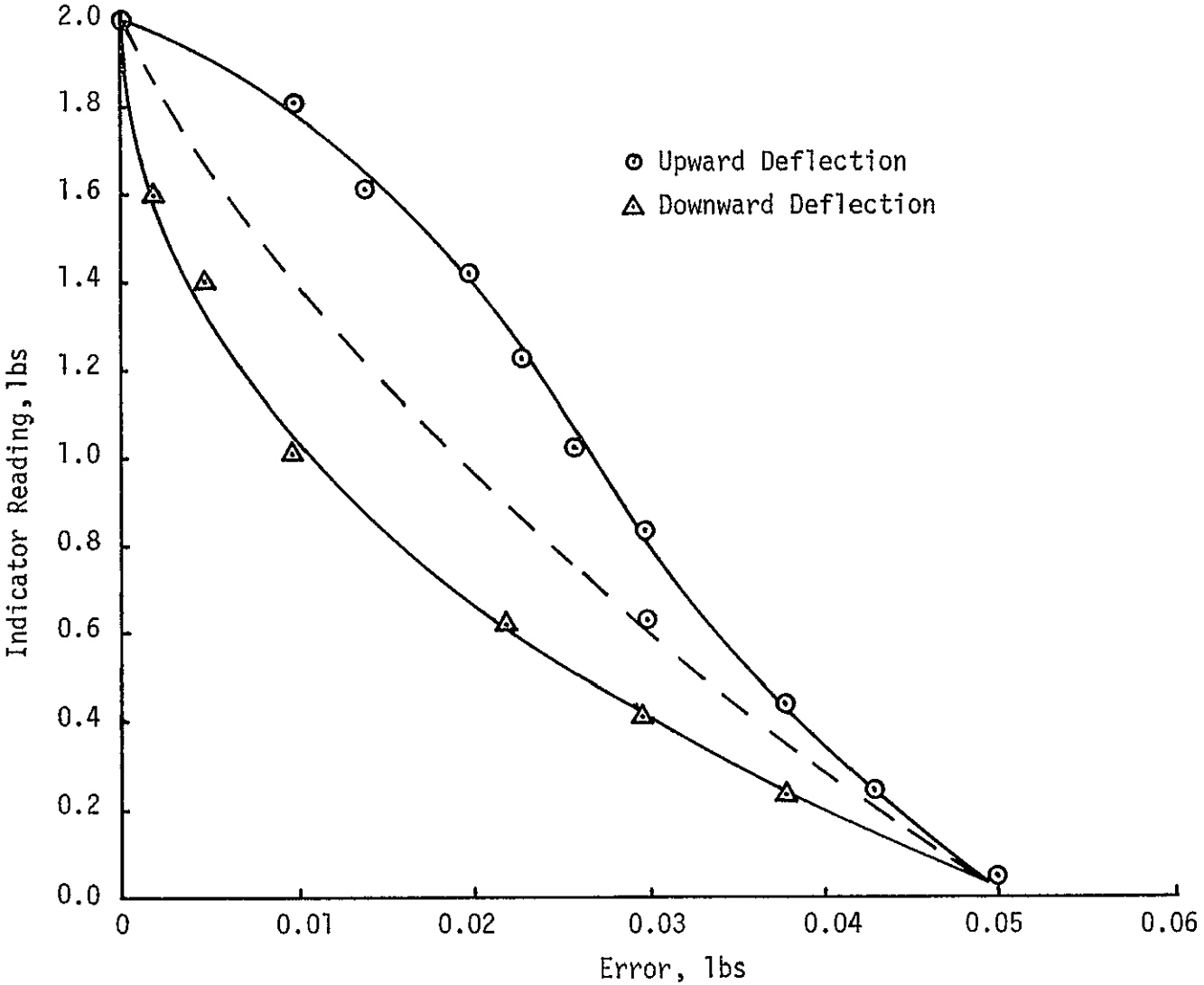

Figure 35. Correction Curve For Scales

Figure 35. An average of these two values was taken and plotted between the two curves and used as the correction factor. The motor was then adjusted to a constant speed and the balance set such that the scale indicated 2.0 lb. This was done for each liquid flowrate to eliminate the affect of momentum on the indicator reading. The photodiode current with clear liquid flowing through the channel was set at 0.40 μa. Nitrogen was introduced into the channel and the scale indicator position read. The initial reading minus the scale indicator reading with two-phase flow plus the correction factor gave the amount of liquid displaced by the nitrogen in the channel. The calibration curves at motor speeds of 400 to 600 rpm are shown in Figure 36.

It should be noted that the low pressure at which the nitrogen was introduced caused channeling, i.e., the nitrogen bubbles tended to adhere to the inside walls of the channel, which caused some error in the calibration. In an effort to prevent this, a small baffle plate was placed above the channel entrance, however, this proved to be ineffective. Other contributing errors could have been the weight of the nitrogen in the exit hose, and the inconsistency of the motor speed due to heating of the rheostat.

It was concluded from this experiment that it is feasible to determine the saturation in a porous matrix through which a two-phase mixture is flowing by measuring

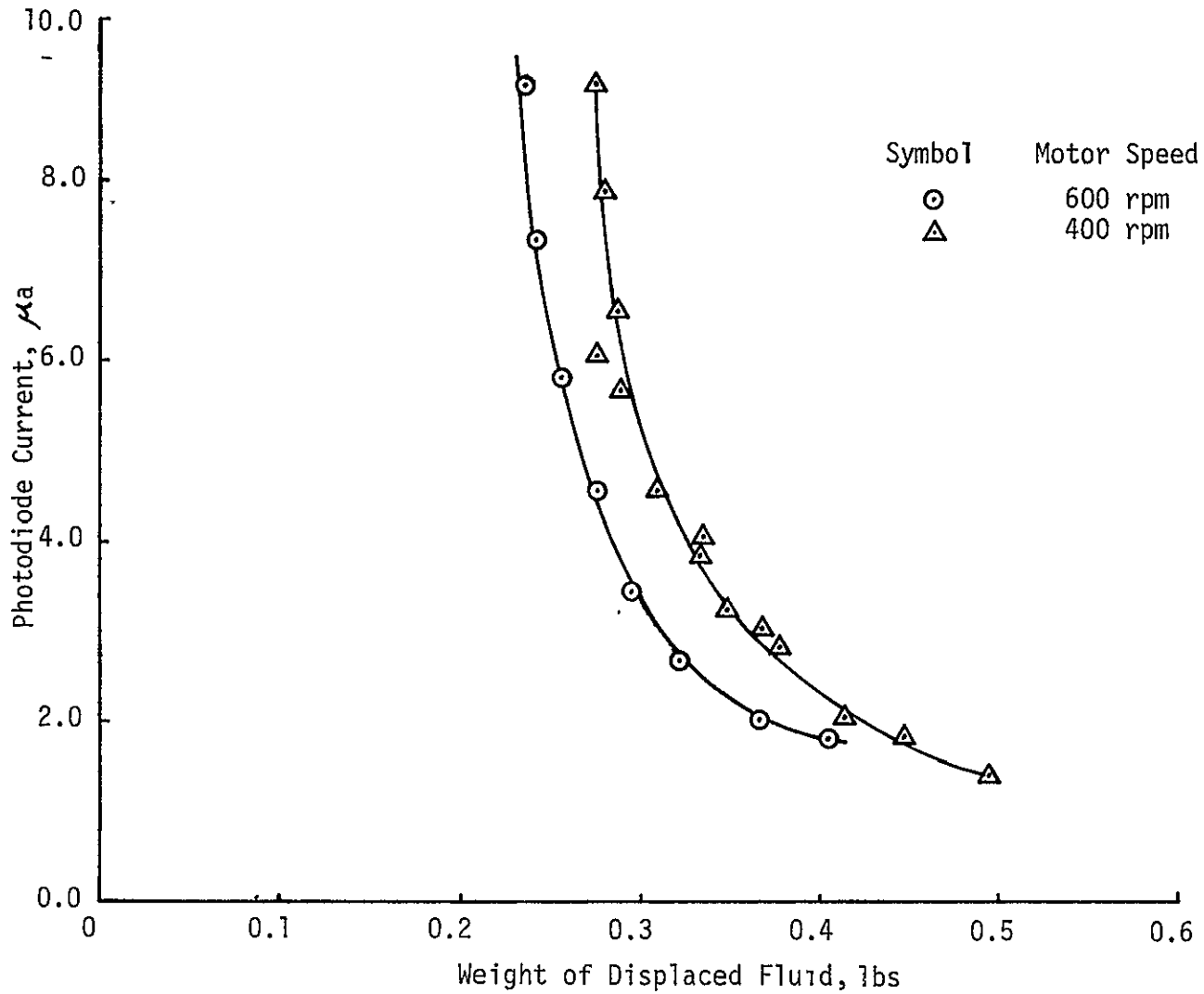

Figure 36. Photodiode Current Versus Weight of Displaced Fluid by Gas

the amount of light dispersed by the porous matrix and two-phase mixture. The procedure for calibrating the meters used in the boiling experiment was refined as a result of findings in this experiment.

LIST OF REFERENCES

1. Argo, W. B. and Smith, J. M. "Heat Transfer in Packed Beds," Chemical Engineering Progress, Vol. 49, (1953), pp. 443-51.

2. Bunnell, D. G., Irvin, H. B., Olson, R. W. and Smith, J. M. "Effective Thermal Conductivities in Gas-Solid Systems," Ind. Eng. Chem., Vol. 41, (1949), p. 1977.

3. Coberly, C. A. and Marshall, W. R. "Temperature Gradients in Gas Streams Flowing Through Fixed Granular Beds," Chemical Engineering Progress, Vol. 47, (1951), p. 141.

4. Collins, Royal Eugene, Flow of Fluids Through Porous Materials, Reinhold Publishing Corporation, New York, 1961, p. 4.

5. Felix, J. R. and Neill, W. K. Preprints Heat Transfer Symposium, Annual meeting American Institute of Chemical Engineers, Atlantic City, (December 1951), p. 125.

6. Geiringer, Paul L. Handbook of Heat Transfer Media, New York, Reinhold Publishing Corporation, 1962.

7. Golpalarathnam, C. D., Hoelscher, H. E. and Laddha, G. S. "Effective Thermal Conductivity in Packed Beds," AIChE Journal, Vol. 7, (1961), p. 249.

8. Henry, H. R. "The Effects of Temperature and Density Gradients Upon the Movement of Contaminants in Saturated Aquifers," Bureau of Engineering Research, University of Alabama, June 1966.

9. Hinschharn, Harry J., Goldsmith, Alexander and Waterman, Thomas E., Handbook of Thermophysical Properties of Solid Materials, Vol. 3, New York: The Macmillan Co., 1961.

10. Irvin, H. B., Olson, R. W. and Smith, J. M. "Design of Fixed-Bed Catalytic Reactors," Chemical Engineering Progress, Vol. 47, (1951), p. 287.

LIST OF REFERENCES (Continued)

11. Keenan, Joseph H. and Keyes, Frederick G., Thermodynamic Properties of Steam, New York: John Wiley and Sons, Inc., 1963.

12. Larkin, R. P., White, R. R. and Jeffrey, D. W., "Pressure Holdup and Liquid Holdup in a Packed Tower," AIChE Journal, Vol. 7, No. 2, (1961), p. 231.

13. Lockhart, R. W., and Martinelli, R. C. "Proposed Correlation of Data for Isothermal Two-Phase, Two Component Flow in Pipes," Chemical Engineering Progress, Vol. 45, (1949), p. 39.

14. Martinelli, R. C. and Nelson, D. B. "Prediction of Pressure Drops during Forced Circulation Boiling of Water," Trans. ASME, Vol. 70, (1948), pp. 699-702.

15. McAdams, W. H. Heat Transmission, Second Edition, New York: McGraw-Hill Book Company, Inc., 1942.

16. McAdams, W. H., Woods, W. K. and Heroman, L. C. Jr., "Vaporization Inside Horizontal Tubes: II Benzene-Oil Mixtures," Trans. ASME, Vol. 64, (1942), pp. 193-200.

17. Owens, W. L. "Two-Phase Pressure Gradient," International Developments in Heat Transfer, Pt. II, (1961), pp. 363-368.

18. Ranz, W. E. "Friction and Transfer Coefficients for Single Particles and Packed Beds," Chemical Engineering Progress, Vol. 48, (1952), p. 247.

19. Sanders, A. O. "Similitude and the Heat Flow Through a Granulated Material," Phil. Mag., xiii, (June 1932), p. 1186.

20. Schotte, William, "Thermal Conductivity of Packed Beds," AIChE Journal, Vol. 6, (March 1960), p. 63.

21. Schuler, R. W., Stallings, V. P. and Smith, J. M. "Heat and Mass Transfer in Fixed-Bed Reactors," Chemical Engineering Progress Symposium Series, Vol. 48, No. 4, (1952), p. 19.

22. Shumann, T. E. W. and Voss, V. "Heat Flow Through Granulated Material," Fuel, Vol. 13, (1934), p. 249.

LIST OF REFERENCES (Continued)

23. Union Carbide Corporation, Chemicals Division, Glycols, 1964.

24. Weekman, Vern W. Jr., and Myers, John E. "Fluid Flow Characteristics of Con-Current Gas-Liquid Flow in Packed Beds," AIChE Journal, Vol. 10, (Nov. 1964), p. 951.

25. Weekman, Vern W. Jr., and Myers, John E. "Heat Transfer Characteristics of Con-Current Gas-Liquid Flow in Packed Beds," AIChE Journal, Vol. 11, (Jan. 1965), p. 13.

END

DATE FILMED

NOV 11 1970